Russian Chemical Reviews **75** (12) 1083 – 1106 (2006) © 2006 Russian Academy of Sciences and Turpion Ltd

DOI 10.1070/RC2006v075n12ABEH003598

The kinetic ordering and growth dissymmetrisation in crystalline solid solutions

A G Shtukenberg, Yu O Punin, O V Frank-Kamenetskaya

Contents

I.	Introduction	1083
II.	Experimental techniques for the elucidation of the growth dissymmetrisation of crystals	1086
III.	The symmetry aspects of the dissymmetrisation and the structural inhomogeneity of crystals	1090
IV.	Dissymmetrisation-induced changes in the crystal structure	1093
V.	The metastability of the kinetic ordering	1095
VI.	The kinetic ordering and the atomic structures of growing faces	1096
VII.	The diffusion relaxation	1097
VIII.	Control factors of the kinetic ordering	1099
IX.	Conclusion	1103

Abstract. The review concerns the order – disorder kinetic (growth) phase transitions, which are characteristic of inorganic crystalline solid solutions. The emphasis is placed on the emergence of metastable low-symmetry phases (*i.e.*, the dissymmetrisation of crystals), which can occur due to the drastic difference between the atomic structures of growing faces and the bulk crystal. The experimental techniques for the elucidation of this phenomenon, possible crystal symmetries and structures induced by the dissymmetrisation as well as the effects of crystal composition, growth medium composition, growth temperature and growth rate are analysed. The bibliography includes 177 references.

I. Introduction

The order – disorder transitions are equally typical of naturally occurring and artificial crystals. The phase diagram of a compound can reveal areas of the thermodynamic stability and instability of its ordered and disordered phases in specific ranges of thermodynamic parameters, *e.g.*, temperature and pressure. A change in the thermodynamic parameters can induce a transition from an ordered into a disordered phase or *vice versa*. Such classical phase transitions have been known for a long time and are beyond the scope of the present review. This review concerns the kinetic (or growth) order – disorder phase transitions.[1,2]

A kinetic phase transition implies the emergence of a phase of a particular compound (with either constant or variable stoichiometry) within the stability range of another phase of the same compound driven by kinetic factors.[3–5] The term 'kinetic phase transitions' emphasises that it is kinetic rather than thermodynamic factors that act as the control parameters for such transitions. Kinetic tranistions in crystals with variable stoichiometry (*i.e.*, solid solutions), which is a particular case of this general phenomenon, can be classified into two groups, *viz.*, ordering and disordering transitions. The former ones occur due to the selective incorporation of solid solution components into different crystallographic sites of a growing crystal face. The latter ones occur due to a poorer statistical selection of different atoms at high crystal growth rates (atoms in the surface layer do not have enough time to settle themselves in the sites corresponding to an ordered state before a next layer is deposited).[1] We limit ourselves to only kinetic ordering processes, since quite extensive experimental data on this subject became available over the recent years.

At the first glance, the kinetic ordering phase transitions look exotic among numerous ordinary equilibrium phase transitions. However, a careful consideration of the issue indicates that these transitions are not so rare, especially, in the case of solution-grown crystals. Presently, this phenomenon has been well documented for $\sim$30 compounds (Table 1 – 3), but we believe that the actual range of its occurrence is far broader and it is characteristic of the majority of solid solutions.

Investigations into the kinetic phase transitions are encouraged by the interest in unusual behaviour of crystals and processes responsible for the formation of crystalline solid solutions. The underlying regulations can be applied to reconstruct conditions of the mineral formation in nature.

Atoms, vacancies and their groups can be a subject of either positional or rotational ordering. The presence of partial occupancies of crystallographic sites statistically occupied by different atoms and vacancies in the crystal structure is a prerequisite to the kinetic positional ordering. This phenomenon can be observed both in the case of complete miscibility of isomorphous components [*e.g.*, the ordering of trivalent cations in garnets of the grossularite – andradite series, $Ca_3(Al,Fe)_2(SiO_4)_3$] and limited isomorphism (as in the case of the ordering of the Al^{3+} cations substituting for the Si^{4+} ions in quartz, SiO_2). The kinetic ordering can take place when a respective ordinary thermodynamic phase transition is both known [*e.g.*, orthorhombic – hexagonal cordierite $Mg_2Al_3(AlSi_5O_{18})$] and unknown [*e.g.*, orthorhombic – triclinic topaz $Al_2SiO_4(OH,F)_2$].

The known cases of the orientational kinetic ordering are rather scarce. In particular, such an ordering in the distribution of the OH groups was described in apophyllite $KCa_4(Si_4O_{10})_2 \cdot (F,OH) \cdot 8\,H_2O$ crystals.[38] Probably, a similar effect is typical of grossularite garnet $Ca_3Al_2[SiO_4,(OH)_4]_3$ crystals.[87,120] Yet

A G Shtukenberg, Yu O Punin, O V Frank-Kamenetskaya Department of Geology, St Petersburg State University, Universitetskaya nab. 7/9, 199034 St Petersburg, Russian Federation. Fax (7-812) 328 44 18, tel. (7-812) 328 96 47, e-mail: sasha@as3607.spb.edu (A G Shtukenberg), crystgen@geology.pu.ru (Yu O Punin), olga@OF3102.spb.edu (O V Frank-Kamenetskaya)

Received 5 October 2005
Uspekhi Khimii **75** (12) 1212 – 1236 (2006); translated by Ya V Zubavichus

another example is given by the orientational ordering in the distribution of the SO_4^{2-} groups revealed for the dissymmetrisation of crystals of aluminium chromium potassium alum, $K(Al,Cr)(SO_4)_2 \cdot 12\,H_2O$.[34] However, these three cases virtually encompass all available information on the orientational kinetic ordering. Therefore, we shall further discuss the positional ordering only.

The early history of investigations into the kinetic ordering of atoms, often also referred to as the growth dissymmetrisation of crystals, dates back to the 1960s, when several compounds featuring the ordered distribution of dopant atoms over specific crystallographic sites equivalent in the parent high-symmetry structure [in particular, the ordering of the Gd^{3+} ions in synthetic corundum Al_2O_3 (Ref. 84) and of the Fe^{3+} ions in calcite $CaCO_3$ (Ref. 85) and amethyst, a purple quartz modification [74, 75]] were discovered. In all these cases, the growth processes were suggested to be the driving factor for the ordering (in particular, the nonequivalence of different sites with respect to the crystal growth front was noted) although no detailed mechanism of this phenomenon was then formulated. The general idea of the growth ordering mechanism was proposed by Shubnikov [121] based on theoretical arguments. For the first time, this mechanism has been elaborated in detail by Tsinober and Samoilovich [79] for quartz and by Nizamutdinov *et al.*[81] for zinc selenate and sodium kröhnkite $Na_2Cd(SO_4)_2 \cdot 2\,H_2O$ (Ref. 80) and somewhat later by Akizuki and Sunagawa [63] for adularia (which is a low-temperature

Table 1. Examples of the growth dissymetrisation in crystalline solid solutions according to diffraction methods.

Solid solution, chemical formula	Growth sector [a]	Ideal space group	Real space groups	Optical anomalies [b]	Signatures in diffraction [c]			Ordering type, maximum degree	Number of structures studied [d]	Ref.
					1	2	3			
Isotropic crystals										
Garnets										
$Ca_3(Al,Fe)_2(SiO_4)_3$	{110}	$Ia\bar{3}d$	$Fddd$, $I\bar{1}$	$\Delta n = 0.015$	+	+	+	Al/Fe, 0.74	9	6–16
$Ca_3(Al,Cr,V)_2(SiO_4)_3$	{110}	$Ia\bar{3}d$	$Fddd$, $I\bar{1}$	$\Delta n = 0.007$	+	+	+	Al/Cr, 0.66	7	17, 18, our data
$(Y,Nd)_3Ga_5O_{12}$	{110}	$Ia\bar{3}d$	?	$\Delta n = 0.0004$	+	?	?	Y/Nd (see [a])	–	19–21
Analcimes-pollucites $Cs_xNa_{1-x}AlSi_2O_6 \cdot (1-x)\,H_2O$	?	$Ia\bar{3}d$	$I4_1/acd$, $Ibca$, $I2_12_12_1$	$\Delta n > 0$	+	+	+	Al/Si, 0.92 Na/□, 0.23 Cs/H_2O, 0.30	8	22–25
$Na(ClO_3,BrO_3)$	{100}, {111}, {$\bar{1}\bar{1}\bar{1}$}	$P2_13$	$P1$, $R3$	$\Delta n = 0.02$	+	+	+	ClO_3/BrO_3, 0.75	20	26–28
Alum										
$K(Al,Cr)(SO_4)_2 \cdot 12\,H_2O$, $(K,NH_4)Al(SO_4)_2 \cdot 12\,H_2O$, other isomorphous series	{111}	$Pa\bar{3}$	$R\bar{3}$, $P\bar{1}$	$\Delta n = 0.0001$	–	+	–	Al/Cr, 0.10 NH_4/K, 0.05	4	29–34, our data
$(Pb,Ba)(NO_3)_2$, $(Pb,Sr)(NO_3)_2$	{111}	$Pa\bar{3}$	$R\bar{3}$, $R3$	$\Delta n > 0$	–	+	+	Pb/Ba, 0.22 Pb/Sr, 0.09	6	35, 36, our data
Uniaxial crystals										
Apophyllite [e] $KCa_4(Si_4O_{10})_2(F,OH) \cdot 8\,H_2O$	{101}, {110}	$P4/mnc$	?	$2V = 88°$	?	?	?	OH^-	6	37–39
Vesuvianite $Ca_{19}(Mg,Fe,Al)_{13}Si_{18}O_{68} \cdot (O,OH,F)_{10}$	{110}, {111}	$P4/nnc$	$P2/n$	$2V = 45°$	+	?	+	Al/Fe, 0.85	6	40–42
Cordierite $Mg_2Al_3(AlSi_5O_{18})$	{10$\bar{1}$0}, {0001}	$P6/mcc$	$Cccm$	$2V = 90°$	+	+	+	Al/Si, 1	∞	43–54
Tourmaline (elbaite-liddicoatite) $(Ca,Na)(Al,Li)_3 \cdot Al_6(Si_6O_{18})(BO_3)_3(OH)_3F$	{10$\bar{1}$1}, {02$\bar{2}$1}, {11$\bar{2}$0} {10$\bar{1}$0}	$R3m$	Cm, $C1$	$2V = 30°$	+	+	+	Al/Li, 0.33	3	55, 56, our data
Edingtonite $BaAl_2Si_3O_{10} \cdot 4\,H_2O$	{110}, {001}	$P\bar{4}2_1m$, $P2_12_12$	$P1$	$2V = 54°$	+	?	?	Al/Si	–	57, 58
bis(11-Bromoundecanoyl) peroxide	{100}	$P4_32_12_1$ $P2_12_12_1$	$P1$	$2V > 0$	?	?	?	molecules	1	39, 59–61
1,5-Dichloro-2,3-dinitrobenzene	{100}	$P4_32_12_1$ $P2_12_12_1$	$P1$	$2V > 0$	?	?	?	molecules, 0.68	2	39
Biaxial crystals										
Adularia $KAlSi_3O_8$	{110}, {1$\bar{1}$0}	$C2/m$	$C\bar{1}$	+	+	+	+	Al/Si	∞	43, 47 62–64
Asparagine-aspartic acid	{010}	$P2_12_12_1$	$P12_11$	–	?	+	?	molecules, 0.13	1	60, 61, 65, 66
Brewsterite $(Sr,Ba)_2Al_2Si_{12}O_{32} \cdot 10H_2O$	{011}, {610} {010}	$P2_1/m$	$P\bar{1}$	+	+	?	?	Al/Si	3	67, 68

Table 1 (continued).

Solid solution, chemical formula	Growth sector [a]	Ideal space group	Real space groups	Optical anomalies [b]	Signatures in diffraction [c]			Ordering type, maximum degree	Number of structures studied [d]	Ref.
					1	2	3			
Biaxial crystals										
Topaz $Al_2SiO_4(OH,F)_2$	{*hkl*}, {*hk*0}	*Pbnm*	*P*1	+	–	?	+	OH/F	1	69 – 72
Yugawaralite $CaAl_2Si_6O_{16}\cdot 4H_2O$	{011}, {120}	*C*2/*m*	*Pc*, *P*1	+	+	?	?	Al/Si	2	58, 73
Cinnamamide-2-thienyl-acryl amide	{001}, {011}	$P2_1/m$	*Pc*, *P*1	–	+	?	+	molecules, 0.73	3	61, 65

Notes. 'Our data' stands for unpiblished crystal structure data by the authors of the present review.
[a] Only the growth sectors that have been characterised by X-ray diffraction or spectroscopic techniques are included; [b] Δn is the maximum birefringence (*i.e.*, the difference between principal values of the refraction index of the crystal), $2V$ is the maximum angle between the optical axes; the presence of optical anomalies (+) in a biaxial crystal can be revealed according to one of the following criteria: the sector zoning in the distribution of optical parameters, a non-typical optical indicatrix, variations of optical properties over the crystal not related to stoichiometry variations; [c] 1 are distortions of the ideal unit cell parameters, 2 are different intensities of reflections, which were symmetry-equivalents in the parent structure, 3 is the appearance of forbidden reflections. The symbols '+'and '–' denote the presence and the absence of the dissymertisation signature, respectively, the symbol '?' means that no information is available; [d] the number of independent crystal structure refinements for a compound in low-symmetry space groups is given; the dash symbol in this column means that no crystal structure refinement has been accomplished and the conclusions on the real symmetry have been derived based on a qualitative analysis of the experimental diffraction pattern; the symbol '∞' indicates that the number of independent refinements is large due to the possibility of equilibrium phase transitions; [e] the orientational ordering of the OH groups have been detected with IR spectroscopy and the growth origin of the ordering has been confirmed by the observation of optical anomalies.

modification of potash feldspar, $KAlSi_3O_8$) and for a series of other compounds, including apatite $Ca_5(PO_4)_3(OH,F)$,[97] garnets,[7] apophyllite,[38] topaz,[69] analcime $NaAlSi_2O_6\cdot H_2O$ (Ref. 23), *etc*.

According to these results, the mechanism of the dissymmetrisation can be described as follows. Crystallographic sites statistically occupied by different atoms and vacancies are strictly equivalent only in the bulk of the crystal. They can well become geometrically and energetically non-equivalent on the crystal surface, which enables their regular occupation by different structural units. The ordered state emerged on the surface can further drift towards the bulk of the crystal. Although this state is metastable, it can be preserved in the crystal for a long time due to very low diffusion rates typical of solids. As a result, the structure of a crystal becomes distorted and its symmetry decreases.

It is known [122] that the crystal growth proceeds as the attachment of atoms, molecules or other building blocks to the crystal surface. The crystal surface can be either atomically smooth or rough at the molecular level. The attachment of atoms to a smooth surface is difficult and thus the growth can be realised only as a tangential movement (*i.e.*, parallel to the face surface) of growth steps (which is the layer-by-layer, or tangential growth), since the attachment of an atom to a step end is much more favourable energetically than that to the flat surface. In the case of a rough surface, atoms can attach to any its point, which gives rise to a uniform movement of the face as a whole (which is the normal growth). Schemes of the emergence of site non-equivalence for the cases of the normal and tangential growth modes are shown in Fig. 1. It is clear that atoms having identical environments in the bulk of the crystal, can occupy sites that are non-equivalent with respect to a face or a face step of the crystal. These two cases give rise to the normal and tangential selectivity of the component incorporation, respectively.

The growth dissymmetrisation is a rather interesting phenomenon from the thermodynamic viewpoint. It is manifested most prominently upon the crystallisation under conditions close to the equilibrium, in particular, at low growth rates. This results in an apparent contradiction to the laws of non-equilibrium thermo-

Table 2. Examples of the growth dissymmetrisation in crystalline solid solutions according to electron spin resonance data.

Compound, chemical formula	Tracedopant	Growth sector	Ideal space group	Real space group	$I_1 : I_2 : I_3 \ldots$	Optical anomalies	Ref.
Quartz, SiO_2	Al^{3+}, Fe^{3+}	{0001}, {$\bar{1}\bar{1}$20}, {01$\bar{1}$1}	$P3_121$	$P3_121$ $P2$ $P1$	1 : 1 : 1 1 : 0.2 : 0.2 1 : 0.2 : 0.1	$2V = 25^\circ$	43, 74 – 79
$ZnSeO_4\cdot 6H_2O$	Cu^{2+}	{102}, {112}, {110}, {001}	$P4_12_12$	$P1$	2 : 1 : 3 : 2.5	$2V > 0$	80 – 83
$Na_2Cd(SO_4)_2\cdot 2H_2O$	Cu^{2+}, Gd^{3+}, V^{4+}	{010}	$P2_1/c$	–	8 : 1	?	80, 82, 83
Corundum Al_2O_3	Gd^{3+}	–	$R\bar{3}c$	–	–	?	84
Calcite $CaCO_3$	Fe^{3+}, Mn^{2+}	–	$R\bar{3}c$	–	–	?	85

Notes. Similar patterns of ordering of paramagnetic defects were also observed in herderite, phenacite and beryl;[86] however, the growth nature of the ordering therein was not elucidated. $I_1 : I_2 : I_3$ is the maximum experimentally measured intensity ratio of the ESR spectral signals that are equivalent in the parent crystal structure.

Table 3. Examples of crystals, for which the growth dissymmetrisation is suspected based on indirect methods.

Compound	Formula	Symmetry class	Ref.
Isotropic crystals			
Garnets grossularite – hydrogrossularite	$Ca_3Al_2[SiO_4,(OH)_4]_3$	$m\bar{3}m$	87
Ralstonite	$Na_xMg_xAl_{2-x}(OH,F)_6 \cdot H_2O$	$m\bar{3}m$	88
Strontium titanate	$SrTiO_3$	$m\bar{3}m$	89
Uniaxial crystals			
Apatite	$Ca_5(PO_4)_3(OH,F)$	$6/m$	90 – 98
Eremeyevite	$Al_6(BO_3)_5(OH)_3$	$6mm$	93, 99 – 102
Calcite	$CaCO_3$	$\bar{3}m$	103
Dolomite	$CaMg(CO_3)_2$	$\bar{3}$	103
Milarite	$K_2Ca_4Be_4Al_2Si_{24}O_{60} \cdot H_2O$,	$6/mmm$	90, 92, 104
Osumilite	$(K,Na)_2(Fe,Mg)_4 \cdot (Al,Fe)_3Si_{24}O_{60} \cdot 2\,H_2O$	$6/mmm$	105, 106
Tourmaline	$Na(Al,Li,Mg,Fe)_3 \cdot Al_6(Si_6O_{18})(BO_3)_3 \cdot (OH,O)_3(OH,F)$	$3m$	90, 93, 107
Chabazite (including herschelite, phacolite)	$Ca_2Al_4Si_8O_{24} \cdot 13\,H_2O$	$\bar{3}m$	90, 108 – 110
Biaxial crystals			
Brookite	TiO_2	mmm	111
Harmotome	$Ba_2Al_4Si_{12}O_{32} \cdot 12\,H_2O$	$2/m$	112
Mesolite	$Na_{16}Ca_{16}Al_{48}Si_{72}O_{240} \cdot 64\,H_2O$	2	113
Natrolite	$Na_{16}Al_{16}Si_{24}O_{80} \cdot 16\,H_2O$	$mm2$	113
Prenite	$Ca_2Al_2Si_3O_{10}(OH)_2$	$mm2$	90, 114
Scolecite	$Ca_8Al_{16}Si_{24}O_{80} \cdot 24\,H_2O$	m	113
Staurolite	$Fe_2Al_9O_7(OH)(SiO_4)_4$	$2/m$	115
Stilbite	$Na_2Ca_4Al_{10}Si_{26}O_{72} \cdot 34\,H_2O$	$2/m$	116, 117
Epidote	$Ca_4(Al,Fe)_6O_2(SiO_4)(Si_2O_7)OH$	$2/m$	118
Epistilbite	$Ca_3Al_6Si_{18}O_{48} \cdot 16\,H_2O$	$2/m$	119

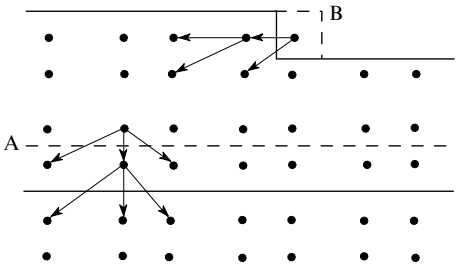


Figure 1. Scheme illustrating the non-equivalence of atoms, which are equivalent in the bulk of a crystal, with respect to the growth front.
A is the normal selectivity case, B is the tangential selectivity case. The solid and dashed lines correspond to two consecutive positions of the crystal growth front; the arrows mark the geometric environment of an atoms at the moment of its incorporation into the crystal (adapted from Ref. 80).

dynamics stating that non-equilibrium structures should emerge far from the equilibrium.[123 – 125] Actually there is no contradiction, since the emergence of non-equilibrium structures concerns the non-linearity of physical and chemical processes related to the deviation from the equilibrium rather than the mere fact of a deviation. Provided that the non-linearity is the strongest at small deviations from the equilibrium (exactly as it occurs upon the specific adsorption of atoms on the surface of a growing crystal), the probability of the emergence of non-equilibrium structures will increase with an approach to the equilibrium.

Over the whole history of investigations into the growth ordering, a large body of information on both the mechanism of the phenomenon and its influence on the symmetry and structure of the resultant crystalline solid solutions has been gathered.

The present review aims at the generalisation and critical analysis of the available data on all aspects of the growth ordering and experimental techniques for its elucidation. The emphasis is placed onto the crystallochemical origins of the growth disymmetrisation.

II. Experimental techniques for the elucidation of the growth dissymmetrisation of crystals

1. Crystal optics

According to the Neumann's principle, a decrease in the symmetry of a crystal should be reflected in the symmetry of its physical properties. In particular, this is valid for crystal optical parameters described by the dielectric impermeability tensor. The dielectric impermeability ψ represents reciprocal dielectric permeability and relates to the refraction index as [126]

$$\psi = n^{-2}.$$

The shape and the orientation of the optical indicatrix, which is the representation surface of this tensor, have to reflect properly the real symmetry of the crystal. The growth dissymmetrisation is accompanied by a change in the optical properties of the crystal, which is manifested in the appearance of characteristic 'optical anomalies'. For instance, the optical indicatrix of a cubic crystal can transform from a sphere to a uniaxial or biaxial ellipsoid, and the initially optically isotropic crystal will become birefringent. The degree of distortion of the optical indicatrix is described by the birefringence, which is the difference between the maximum and the minimum refraction indices.

Crystal optical methods have several evident advantages over alternative methods for the elucidation of the growth ordering. These include the high sensitivity to minute distortions of the crystal structure induced by ordering of structural units; the possibility of simultaneous monitoring of crystal optical parameters over a large number of the crystals under study; the straightforwardness and affordability of the analysis: the analysis of a large amount of samples does not require long time and expensive instrumentation. Thus the crystal optics is indispensable at preliminary stages of the investigation, *i.e.*, for the detection of the dissymmetrisation and for the quantification of the degree of this effect within a number of samples from the same isomorphous series. Overall, the method does not allow one to establish what types of crystal structure distortions are responsible for the observed distortions of the optical indicatrix. However, some robust algorithms for rather accurate calculations of the optical indicatrix based on the crystal structure have been elaborated recently.[127 – 134] By performing calculations and comparing theoretical optical parameters with the experimental ones for a series of models one can analyse the origin of the optical anomalies with their relation to the ordering of structural units. In particular, such calculations were performed for garnets of the grossularite – andradite $Ca_3(Al,Fe)_2(SiO_4)_3$ (Refs 14 – 16) and grossularite – uvarovite $Ca_3(Al,Cr)_2(SiO_4)_3$ series (Refs 15 and 16) and for sodium chlorate bromate [28] (Fig. 2).

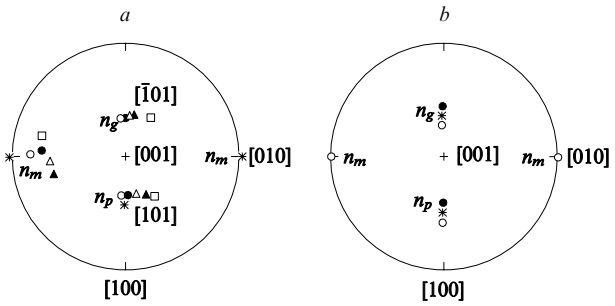


Figure 2. Theoretical (dots) and experimental (asterisks) orientations of the optical indicatrix for garnets of the grossularite – uvarovite isomorphous series (*a*) and sodium chlorate bromate crystals [28] (*b*);
n_m, n_p and n_g are the principal values of the refraction index of a crystal; different data points correspond to different samples; the experimental crystal optical parameters and atomic coordinates used in the calculations were taken from the Refs 17 and 28 for *a* and *b*, respectively.

2. Electron spin resonance

The kinetic ordering of atoms in a crystal has been detected for the first time using electron spin resonance (ESR). This method is extremely sensitive and makes it possible to reliably measure the concentration of dopant atoms in any specific site of a regular system of points. The major limitations of the method are as follows: the substituting ion should be paramagnetic (or should form a paramagnetic centre); the concentration of the ion should be sufficiently low (below ‰); no other paramagnetic ions should be present in the crystal in high concentrations.

Let us consider a few examples of the application of this method to studies of the dissymmetrisation (see Table 2). Upon the aluminium substitution for the silicon atoms in the crystal structure of quartz (the point symmetry group 32), the $[AlO_4]^{5-}$ complex can lose an electron giving rise to a hole centre, which can easily be detected with ESR. The concentration of the hole centres is directly proportional to the aluminium concentration (and that of respective counter-ions), so that signal intensities in the ESR spectra give information on the fraction of aluminium atoms in various silicon sites. In an ESR study of crystals of artificial smoky quartz, it was found that groups of signals corresponding to the oxygen atoms of different SiO_4 tetrahedra are characterised by different intensities [79] (Fig. 3). For the growth sectors of rhombohedral faces (face symmetry 1), all three groups of signals have different intensities; for the growth sectors of prismatic faces (face symmetry 2), only two groups of signals have identical intensities; and for the growth sectors of pinacoidal faces (face symmetry 3), all three groups of signals have identical intensities. Since the intensity of lines in ESR spectra is directly proportional to the concentration of hole centres, the ordering of the hole centres revealed in this way confirms the dissymmetrisation.

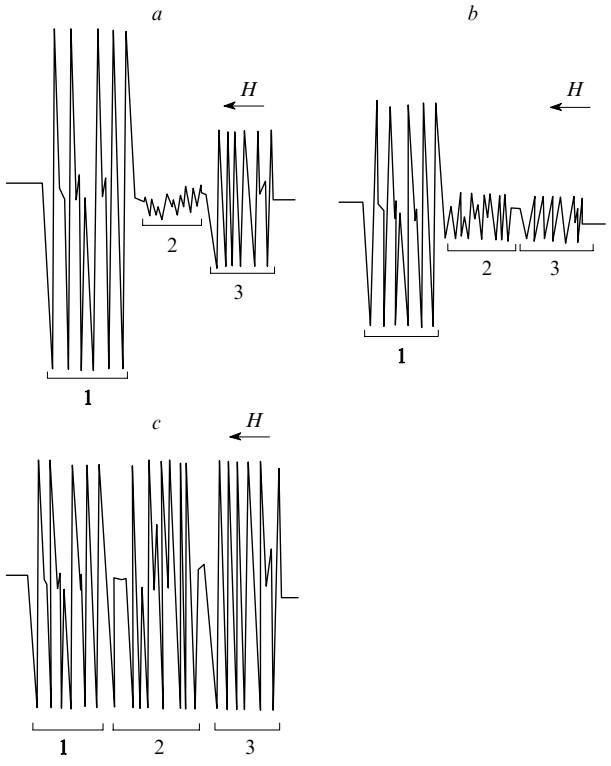


Figure 3. ESR spectra of hole centres in smoky quartz.[79]
The growth sectors: {01$\bar{1}$1} (*a*), {$\bar{1}\bar{1}$20} (*b*) and {0001} (*c*). Groups of signals which have identical intensities in the parent trigonal crystal structure of quartz are denoted with numbers from 1 to 3.

3. Infrared and Raman spectroscopy

Infrared (IR) spectroscopy was successfully applied to the analysis of ordered distribution of the fluoride and hydroxide anions in topaz,[71, 72] the silicon and aluminium cations in adularia [63] and of the orientational ordering of the OH groups in grossularite [120] and apophyllite.[38] Typically, site occupancies cannot be determined by this method, however, it gives information on the presence and the degree of ordering of atoms or atomic groups in the structure.

Unfortunately, the sensitivity of IR spectroscopy is rather low. In particular, several attempts at the detection of the ordering of the Al/Fe atoms in garnets of the grossularite – andradite isomorphous series using this method failed,[11, 12] although it was reliably established using X-ray crystallography by several authors.[6, 16] It is of note that one of the samples studied by X-ray crystallography [6] was studied later by IR and no ordering was revealed.[12] Nevertheless, inclusions of a substantially ordered phase dispersed in a disordered matrix can be efficiently revealed by IR (at sizes far below the detection limit of diffraction techniques).[135]

4. Electron microscopy

High-resolution transmission electron microscopy (HRTEM) as well as other modifications of electron microscopy (*e.g.*, TEM, SEM) can reveal the growth ordering in crystals provided that it is significant and gives rise to strong structural distortions or the appearance of superstructures. The detection of Al/Si ordering in cordierite [135] and prenite $Ca_2Al_2Si_3O_{10}(OH)_2$,[114] Ca/Mg ordering in calcite $CaCO_3$ and dolomite $CaMg(CO_3)_2$ (Ref. 103) can be given as examples of successful applications of electron microscopy.

5. Diffraction methods

It is X-ray, electron and neutron diffraction studies on single crystals (see Table 1) that provide the highest efficiency in the analysis of the nature of the kinetic ordering of atoms in crystals revealing detailed information on the occupancies of crystallographic sites and interatomic distances. In some cases, changes in the ordering can also be tracked by powder X-ray diffraction by monitoring shifts, splitting or broadening of diffraction reflections or the appearance of additional superstructure reflections in the diffraction patterns. In particular, dissymmetrisation-induced changes in the powder diffraction patterns were observed for cordierite $Mg_2Al_3(AlSi_5O_{18})$ [45, 46] and edingtonite $BaAl_2Si_3O_{10} \cdot 4\,H_2O$.[57]

As a rule, the degree of the growth ordering of atoms is low and the lower-symmetry structure subject to refinement is close to the parent high-symmetry one and thus it is difficult to unambiguously establish the fact of a symmetry lowering based on a routine experiment. To provide reliable conclusions on the man-

ifestation and the nature of the dissymmetrisation, it is necessary to collect an accurate set of intensities of diffraction reflections, then carefully analyse the experimental diffraction pattern and refine the crystal structure first in the parent high-symmetry group and then in some of its subgroups selected according to the results of the diffraction pattern analysis.

Recommendations on the accurate measurement of intensities of X-ray diffraction reflections are given elsewhere.[25, 136] In particular, it is advisable to use nearly spherical crystals and collect the whole set of intensities over the entire Ewald sphere rather than only in its symmetry-independent part.

The following signatures of the dissymmetrisation can be observed in a diffraction pattern: distortions of the unit cell dimensions (typically, insignificant ones); differing intensities of reflections equivalent in the ideal space group; the emergence of reflections forbidden in the ideal space group. The logic of an analysis of the crystal dissymmetrisation based on the diffraction pattern can be demonstrated using garnets of the grossularite–andradite isomorphous series (grandites) with a common stoichiometry $X_3Y_2(SiO_4)_3$ (X = Ca, Y = Al, Fe, the ideal space group is $Ia\bar{3}d$). The anomalous birefringence in these crystals is well known.[7, 13, 90] The idea that the optical anomalies in garnets originate in the atomic ordering has been formulated for the first time by Yoder.[137] However, the questions on the presence and the nature of the ordering in garnets remained unanswered until recent years, despite numerous attempts at revealing this ordering using X-ray crystallography undertaken over the last 25–30 years.[6, 8–10, 14–17, 138, 139]

Let us illustrate this approach by the example of a study of three natural grandite crystals (the gtowth sector of rhombododecahedral faces {110}). The parameters of these crystals and the structure refinement results obtained for them by means of X-ray crystallography are summarised in Tables 4 and 5 (for details, see Ref. 16).

Significant deviations from cubic symmetry are observed for two out of three samples. These are manifested in a deviation of one of the angles (β) from 90° (see Table 4), which indicates that the actual symmetry of the crystals is orthorhombic or lower.

For a comparative analysis of the reflection intensities, all reflections equivalent in the ideal cubic diffraction class $m\bar{3}m$ were subdivided into groups according to the symmetry elements of this class. A symmetry element was considered to be violated, if the difference $I_{max} - I_{min}$ between the strongest and the weakest reflections within the respective group exceeded a preset threshold value [in this particular case, it was twice the difference between the intensities of the Friedel equivalents $2\left(I_{hkl} - I_{\bar{h}\bar{k}\bar{l}}\right)_{max}$].

In this way, the fractions P of reflections violating specific symmetry elements of the cubic structure were determined for each group (Fig. 4). It is evident that for the crystal Bazh1, all symmetry elements of the parent point symmetry group are violated to a small virtually constant extent. These violations can be regarded as a background level induced by multiple scattering events, non-ideal spherical shape of the sample and resultant anisotropic absorption of X-rays in the crystal, *etc*. Meanwhile, the symmetry element violations are more prominent for other two crystals. And it is important that different symmetry elements are violated to different extents. In particular, the symmetry planes (010), (101) and ($\bar{1}$01) are violated not as significantly as symmetry axes. This trend is especially prominent for the crystal Bazh2: the symmetry planes therein are violated insignificantly, to an extent comparable to that in Bazh1 with simultaneous substantial violation of the remaining symmetry elements. This gives strong evidence that the crystal Bazh2 is actually orthorhombic. In the case of the crystal Mali, the violation of the symmetry planes is more pronounced, which indicates that the actual symmetry of the crystal is lowered further to triclinic.

An analysis of the systematic absences revealed 12, 391 and 196 reflections forbidden in the ideal space group $Ia\bar{3}d$ for the crystals Bazh1, Bazh2 and Mali, respectively (Table 6). Further-

Table 4. Parameters of three birefringent grandites (Bazh1, Bazh2 and Mali) studied with single-crystal X-ray diffraction.

Parameter	Bazh1	Bazh2	Mali
Fe / (Fe + Al)	0.078	0.58	0.23
Colour	light pink	brown	puce
Δn (see [a])	0.0002(1)	0.0089(1)	0.0066(1)
Refined triclinic unit cell parameters			
a_{tr} /Å	11.856(4)	11.984(2)	11.892(2)
b_{tr} /Å	11.853(4)	11.979(2)	11.889(2)
c_{tr} /Å	11.857(4)	11.980(2)	11.892(2)
α /deg	90.00(0)	90.00(2)	90.00(2)
β /deg	90.00(3)	90.29(2)	90.12(2)
γ /deg	90.00(0)	89.99(2)	90.03(2)
$\langle a \rangle$ /Å	11.855	11.981	11.891

[a] Birefringence value.

Table 5. Parameters of X-ray diffraction measurements and structure refinement for the three birefringent grandites.

Parameter	Bazh1	Bazh2	Mali
Radius of the spherical sample /mm	0.100	0.135	0.150
ρ_{exp} /g cm^{-3}	3.597(4)	3.703(2)	3.698(4)
Diffractometer	Nicolet P3/R3	Nicolet P3/R3	Syntex $P2_1$
$\left(\frac{\sin\theta}{\lambda}\right)_{max}$	0.807	0.807	0.994
μ /cm^{-1}	27.91	42.54	33.94
Number of observed reflections ($I > 2\sigma_I$)	8065	10 619	9238
Number of independent reflections ($F > 4\sigma_F$)			
space group $Ia\bar{3}d$	314	325	482
space group $Fddd$	1853	1904	2193
space group $I\bar{1}$	–	7002	6773
R (%)			
space group $Ia\bar{3}d$	2.81	2.64	4.49
space group $Fddd$	4.36	2.74	3.44
space group $I\bar{1}$	–	3.70	3.26
R_w (%) (see [a])			
space group $Ia\bar{3}d$	4.97	4.94	6.02
space group $Fddd$	5.16	4.63	3.82
space group $I\bar{1}$	–	5.07	3.80

[a] The weighting scheme utilised: $w = 1/[\sigma_F^2 + kF_{obs}^2]$, $k = 0.0010 - 0.0068$.

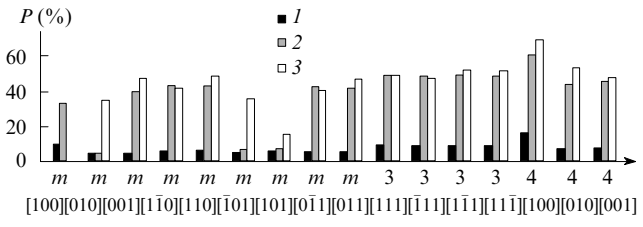


Figure 4. Fractions of diffraction reflections with $I > 4\sigma_I$ violating the symmetry elements of the point symmetry group $m\bar{3}m$ for the three grandite crystals.[15]
(*1*) Bazh1, (*2*) Bazh2, (*3*) Mali.

Table 6. Reflections violating the systematic absences for the space group $Ia\bar{3}d$ observed in the grandite crystals.

Group of reflections	Reflection conditions in the space group $Ia\bar{3}d$	Bazh2			Mali
		total	verified by ψ-scans	approved by ψ-scans [fraction (%)]	total
hkl	$h + k + l = 2n$	0	–	–	0
0*kl*	$k = 2n, l = 2n$	105	22	19 (86%) [a]	36
*h*0*l*	$h = 2n, l = 2n$	5	5	0	7
*hk*0	$h = 2n, k = 2n$	107	11	9 (82%) [a]	49
hhl	$2h + l = 2n$	81	22	13 (59%) [a]	41
hkh	$2h + k = 2n$	12	12	0	28
hkk	$2k + h = 2n$	81	16	10 (63%) [a]	35
Total		391 (4%) [b]	88	51	196 (2%) [b]

[a] With respect to the number of verified reflections. [b] With respect to the total number of relfections.

more, it was shown that the vast majority of the forbidden reflections originate from the structure dissymmetrisation rather than in multiple scattering effects for the latter samples, Bazh2 and Mali.[16, 140] To the contrary, all 12 forbidden reflections in the crystal Bazh1 were shown to be related to multiple scattering, which means that the crystal structure remains cubic.

The preliminary conclusions on the dissymmetrisation of the crystals derived from the analysis of the diffraction patterns can be further proven by the refinements of the crystal structure in all possible space groups, including the ideal one. As a result of this laborious analysis not only the crystal symmetry can be reliably established, but also the nature of the dissymmetrisation can be revealed based on the information on occupancies of crystallographic sites and respective interatomic distances.

The crystal structure refinements were performed according to the standard procedure. The structure was refined by the least-squares method based on an analysis of the difference Fourier maps. A particular attention should be paid to the refinement of site occupancies, since severe errors can appear due to mutual correlations between the occupancies and other variables (primarily, thermal parameters). In order to suppress the effects of these correlations, the following techniques can be applied:[25] the average stoichiometry of the crystal can be constrained; a series of models with fixed occupancies set at several systematically varying values can be refined and compared; the occupancies can be refined against a part of the reflection array including the reflections observed at smaller diffraction angles 2θ, which are less sensitive to uncertainties in the thermal factors. Furthermore, it is often advisable first to place only one of the principal elements into the site with suspected ordering and refine its occupancy without any constraints.

The retrieval of accurate and reliable site occupancies for crystals of solid solutions from experimental diffraction data is a non-trivial task, which can be solved in a correct way not in all cases [see also a discussion of this problem elsewhere [141–144] for the case of the determination of magnesium and iron occupancies in sites M1 and M2 from the crystal structure refinement of olivines $(Mg,Fe)_2(SiO_4)$]. A survey of the experimental data on a number of inorganic compounds indicates [25] that a change in the site occupancy can be reliably detected by means of X-ray crystallography only provided that $\Delta e/\sum e > 0.004$, where Δe is the change in the electron count upon the change in the occupancy of a site taking into account its multiplicity, and $\sum e$ is the total number of electrons in a unit cell.

Table 7. Mean bond lengths and occupancies of the octahedral sites YO_6 in the crystal structures of the non-cubic garnets.

Octahedral site	Sample Bazh2		Sample Mali	
	$\langle Y-O\rangle$ /Å	x_{Fe}	$\langle Y-O\rangle$ /Å	x_{Fe}
Space group *Fddd*				
Y1	2.003(2)	0.861(5)	1.956(5)	0.344(6)
Y2	1.962(2)	0.308(5)	1.935(5)	0.052(6)
Y1 – Y2	0.041	0.557	0.021	0.292
Space group $I\bar{1}$				
Y11	2.004(3)	0.830(5)	1.964(5)	0.471(5)
Y12	2.002(3)	0.830(5)	1.946(5)	0.241(5)
Y13	2.003(3)	0.868(5)	1.951(5)	0.258(5)
Y14	2.004(3)	0.878(5)	1.961(5)	0.340(5)
$(Y1i)_{av}$	2.003	0.852	1.956	0.328
$(Y1i-Y1j)_{max}$	0.002	0.048	0.018	0.230
Y5	1.962(3)	0.277(5)	1.934(5)	0.073(5)
Y6	1.959(3)	0.279(5)	1.938(5)	0.126(5)
Y7	1.960(3)	0.308(5)	1.935(5)	0.032(5)
Y8	1.962(3)	0.320(5)	1.933(5)	0.00(1)
$(Y2i)_{av}$	1.961	0.296	1.935	0.058
$(Y2i-Y2j)_{max}$	0.003	0.043	0.005	0.126

For the example under consideration, the symmetry lowering for the crystals Bazh2 and Mali was shown to be related to the ordering of the iron and aluminium cations in the octahedral sites Y, which is accompanied by a change in the respective mean cation – oxygen bond lengths $\langle Y-O\rangle$ (Table 7). Only one symmetry-independent Y site is present in the parent cubic garnet (space group $Ia\bar{3}d$), whereas this number increases to two and eight in the orthorhombic (space group *Fddd*) and triclinic (space group $I\bar{1}$) structures, respectively.

In general, the more thorough crystal structure refinement confirms the preliminary conclusions derived from the aforementioned analysis of the diffraction pattern. According to the results of X-ray diffraction (Table 8), the crystal Bazh1 is characterised by the cubic symmetry (space group $Ia\bar{3}d$). Small distortions of the cubic symmetry revealed by crystal optical studies lie beyond the detection limit of X-ray crystallography. The crystal Bazh2 is characterised by the orthorhombic symmetry (space group *Fddd*), whereas the sample Mali is triclinic (or pseudoorthorhombic, space group $I\bar{1}$ or $I1$).

Table 8. Symmetry parameters of the grandite crystals.

Parameter	Bazh1	Bazh2	Mali
System			
optical indicatrix orientation	orthorhombic or lower	orthorhombic or lower	orthorhombic or lower
unit cell	cubic	the same	the same
Diffraction class [a]	cubic $m\bar{3}m$	orthorhombic *mmm*	triclinic $\bar{1}$
Space group			
according to systematic absences	$Ia\bar{3}d$	*Fddd*	$I\bar{1}$ or $I1$
according to crystal structure refinement	$Ia\bar{3}d$	*Fddd*	$I\bar{1}$

[a] An analysis of intensities of relfections equivalent in the diffraction class $m\bar{3}m$.

III. The symmetry aspects of the dissymmetrisation and the structural inhomogeneity of crystals

According to the Curie's principle,[126] the symmetry of a crystal during dissymmetrisation should be determined by the symmetry of a growing face (normal selectivity of component incorporation) and(or) face step (tangential selectivity of component incorporation). The intersection of the point symmetry group of a crystal with the point symmetry group of the matter flow normal to the face of a growing crystal (which is the cone symmetry, *i.e.*, the limiting symmetry class ∞mm) gives 10 groups possible for the normal selectivity in the component distribution (for the case of the normal growth mode by the movement of faces), *viz.*, 1, 2, 3, 4, 6, *m*, 2*mm*, 3*m*, 4*mm* and 6*mm*. The respective intersection of the point symmetry group of a crystal with the point symmetry group of the planar matter flow towards a face step (the symmetry class *m*) gives only two point groups possible for the growth mode by the tangential movement of face steps, *viz.*, 1 and *m*.[121]

This simple (and thus rather useful) approach to the description of the crystal symmetries was applied to analyse the dissymmetrisation in many minerals, including analcime $NaAl.Si_2O_6 \cdot H_2O$,[23] grossularite $Ca_3Al_2[SiO_4,(OH)_4]_3$,[87] chabazite $Ca_2Al_4Si_8O_{24} \cdot 13\,H_2O$,[108] sodium chlorate bromate [26] and others. In particular, it was established [69] that upon the dissymmetrisation of topaz crystals (the symmetry class *mmm*), the growth sectors of the pinacoidal faces {010} remain orthorhombic (the 2D symmetry group of these faces is 2*mm*), the growth sectors of the rhombic prismatic faces {*hk*0} become monoclinic (the symmetry group of the faces is *m*), whereas the growth sectors of the rhombic bipyramidal faces {*hkl*} become triclinic (the symmetry group of the faces is 1). Hereinafter, the indices *h*, *k* and *l* in the notations of simple forms,† growth sectors and faces define the inclination of the faces with respect to the coordinate axes *X*, *Y* and *Z* and thus should be small integers.

It has to be noted that the theoretically suggested symmetry lowering is not realised in all cases, since this approach does not take into account the intrinsic symmetry of the atomic sites subject to ordering. There can be no growth ordering, but if it is actually realised, it obeys the above scheme. For instance, under the conditions of the normal selectivity for the cubic faces {100} of alum crystals (the symmetry class $m\bar{3}$), the symmetry of the growth sector formed by this face should be lowered to orthorhombic 2*mm*, however, this growth sector remains cubic in reality (see below).

† A simple form is a set of faces related to each other through the symmetry operations of the point symmetry group,[145] a growth sector (or growth pyramid) of a face is the area within a crystal formed by the growth of this crystal face.

The crystal dissymmetrisation effects can be strictly addressed within the formalism of the Wittke–Garrido colour symmetry groups. Such an approach has been used for the first time by Vinokurov *et al.*[80, 82, 83, 86, 146] to describe the dissymmetrisation in zinc selenate and sodium kröhnkite $Na_2Cd(SO_4)_3 \cdot 2\,H_2O$. The group properties are analysed at a point group level with the explicit consideration of the intrinsic symmetry of the sites involved. The post-dissymmetrisation symmetry of the crystal and the crystallographic sites subject to variable occupancies with isomorphous atoms are obtained as a result of this theoretical analysis.

Such an approach can be illustrated with an analysis of the symmetry of mixed alum crystals $A^+M^{3+}(SO_4)_2 \cdot 12\,H_2O$ (A = K, NH_4, Rb, ...; M = Al, Fe, Cr, ...) (Table 9). Ideally, alum crystals are crystallised in the cubic system with the point symmetry group $m\bar{3}$ but they exhibit optical anomalies originated from the kinetic atomic ordering. Let us consider the ordering of isomorphous atoms in the A^+ or M^{3+} cationic sites [which are the special Wyckoff positions 4(b) and 4(a), respectively]. It is clear that the actual symmetry of the optical indicatrix is compatible with a symmetry lowering due to the growth ordering of the A^+ or M^{3+} cations. Furthermore, it can be seen that in the majority of cases, the theory group analysis predicts the same optical symmetry as does the analysis of the symmetry of a growing face or a face step. In particular, the normal growth of octahedral faces (the 2D symmetry group of this face is 3 within the symmetry class $m\bar{3}$) gives rise to the trigonal symmetry. Meanwhile, the tangential growth of steps on octahedral faces (the step symmetry group is 1) results in the triclinic symmetry. Notwithstanding, as has been mentioned above, the two approaches make sometimes different predictions. For instance, the growth sector of cubic faces should be characterised by the orthorhombic symmetry 2*mm* according to the 2D symmetry group of this face but the group theory analysis predicts the retention of the cubic symmetry for the case of the normal selectivity, and the actual optical indicatrix remains spherical (*i.e.*, no dissymmetrisation occurs).

Therefore, the symmetry of the growth front (*i.e.*, of a crystal face or a face step in the cases of the normal and tangential growth modes, respectively) strongly affects the symmetry of the resultant crystal. The vast majority of crystals are shaped by a set of faces belonging to one or a few regular forms, which enables the spatially inhomogeneous distribution of areas corresponding to different symmetries and structures over a crystal. Possible types of the spatial inhomogeneity commonly evidenced by optical anomalies are considered in detail below.

1. Sector zoning

During the crystal growth, every face forms its own growth pyramid (or sector) and, ideally, any crystal can be represented as a set of pyramids with a common vertex in the centre of the

Table 9. Occupancies of systems of translationally related sites (x_i, $i = 1, 2, \ldots, 4$) and the real symmetry of different growth sectors of alum crystals (symmetry class $m\bar{3}$) according to optical investigations.

Growth sector	Normal selectivity			Tangential selectivity			Observed optical indicatrix symmetry
	site occupancies	face symmetry	assumed optical symmetry	site occupancies	face step symmetry	assumed optical symmetry	
{111}	$x_1 \neq x_2 = x_3 = x_4$	3	uniaxial, normal to (111)	$x_1 \neq x_2 \neq x_3 \neq x_4$	1	triclinic	biaxial, close to uniaxial
{110}	$x_1 = x_2 \neq x_3 = x_4$	*m*	monoclinic	$x_1 = x_2 \neq x_3 = x_4$ (see [a])	*m*	monoclinic or triclinic	biaxial
{100}	$x_1 = x_2 = x_3 = x_4$	2*mm*	cubic	$x_1 = x_2 \neq x_3 = x_4$	*m*	monoclinic	often isotropic, sometimes biaxial

[a] In the present case, the resultant symmetry depends on the orientation of growth steps: if a step is not perpendicular to the symmetry plane, then all the occupancies are different, and the point symmetry group is $\bar{1}$.

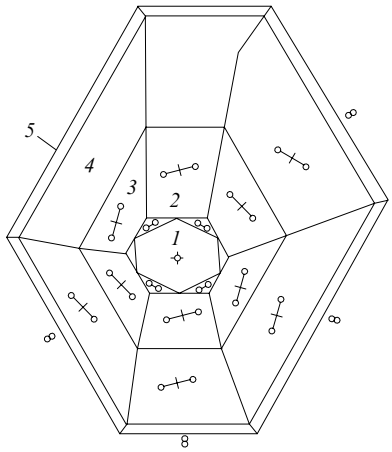


Figure 5. Optical sector zoning in a plate of an eremeyevite $Al_6(BO_3)_5(OH)_3$ crystal cut parallel to the (0001) crystallographic plane.[102]
The growth sectors: (*1*) pinacoid (the angle $2V = 0°$), (*2–4*) hexagonal bipyramids (the angle $2V = 3°$), (*5*) hexagonal prism (the angle $2V = 10–18°$).

crystal and bases coinciding with the crystal external faces. Every growth sector features its own symmetry and crystal structure. The sector growth of different simple forms can be characterised by totally different structures, whereas the structures of different faces belonging to the same regular form can be identical but differently oriented with respect to the common coordinate system, which is similar in some aspects to the twinning texture. This type of the spatial inhomogeneity is a very common signature of the growth dissymmetrisation and, in a sense, can be regarded as its visiting card (for details, see elsewhere [7, 14, 33, 69, 73, 79]). As an illustration, Fig. 5 depicts different orientations of the optical indicatrix for various growth sectors of an eremeyevite crystal.[102] Table 10 lists data on the distribution of optical anomalies over different growth sectors in garnet $Ca_3(Al,Fe,Cr)_2(SiO_4)_3$ crystals.

2. Subsector zoning

The optical sector zoning is often complicated by additional inhomogeneity of the crystal at a subsector level. The term 'subsector zoning' means that several subsectors can be recognised within every growth sector, which are specific areas characterised by their own structures and physical properties. Subsectorial ordering changes are a finer effect as regards the sectorial inhomogeneity, thus its manifestation has only been registered with crystal optical techniques. The reason for the emergence of the subsector zoning is as follows. Growth steps spread out over a crystal face from point sources, *viz*., surface ends of screw dislocations. This is accompanied by the formation of growth (or vicinal) hillocks on the initially flat crystal faces, while the exact shape of the hillocks depends on the anisotropy of the crystal growth rates along the respective steps. The majority of crystals prone to the dissymmetrisation grow from mother liquors following the spiral dislocation mechanism. Since the steps originating from different sides of a vicinal hillock are differently oriented, the crystal areas derived from them under the conditions of the tangential selectivity in the incorporation of isomorphous atoms will appear differently ordered. As a consequence, the distribution of the growth ordering over subsectors formed by differently oriented steps within a sector will reflect the shape of the vicinal hillock.

In particular, typically, vicinal hillocks on the octahedral faces {111} of alum crystals (the symmetry class $m\bar{3}$) have a shape of a trigonal pyramid. As a result, every hillock gives rise to three equivalent subsectors, since the octahedral faces within this symmetry class are characterised by the point symmetry 3. Indeed, the growth sector of the octahedral faces {111} often appears subdivided into three subsectors (derived from one growth hillock) or several triplets of subsectors (derived from different growth hillocks) with different orientations of the optical indicatrix, as can be seen in crystal cuts parallel to the respective growth face. Normally, the subsectors converge in a single point corresponding to the top of the vicinal hillock [33] (Fig. 6). Similar subsector zoning patterns are observed in apatite [97] (Fig. 7), garnets of the grossularite–andradite series,[7] analcime $NaAlSi_2O_6 \cdot H_2O$,[23] chabazite $Ca_2Al_4Si_8O_{24} \cdot 13\,H_2O$,[108] edingtonite $BaAl_2Si_3O_{10} \cdot 4\,H_2O$ [57] and in other crystals. In all these cases,

Table 10. Experimental parameters of the optical indicatrix in different growth sectors for garnet crystals of the $Ca_3(Al,Fe,Cr)_2(SiO_4)_3$ series (the ideal symmetry class is $m\bar{3}m$). Data from Refs 13, 15, 18, 90, 139, 147.

Growth sector	Point symmetry group	Observed optical indicatrix	Theoretical optical indicatrix	Distribution of occupancies of the octahedral sites
Cube {100}	4*mm*	sphere	sphere	$x_1 = x_2 = x_3 = x_4 = x_5 = x_6 = x_7 = x_8$
Octahedron {111}	3*mm*	uniaxial ellipsoid, the optical axis is normal to the (111) face	uniaxial ellipsoid, the optical axis is normal to the (111) face	$x_1 = x_5 \neq x_2 = x_3 = x_4 = x_6 = x_7 = x_8$
Rhombodo-decahedron {110}	2*mm*	biaxial ellipsoid, $n_g \parallel [\bar{1}01]$; $n_m \parallel [010]$; $n_p \parallel [101]$ (face normal)	biaxial ellipsoid, the principal axes are parallel to [010] and $[\bar{1}01]$ and normal to (101)	$x_1 = x_4 = x_5 = x_6 \neq x_2 = x_3 = x_7 = x_8$
Tetragontri-octahedron {211}	*m*	biaxial ellipsoid, $n_p \parallel [211]$ (face normal); the plane defined by the optical axes is parallel to the symmetry plane *m*	biaxial ellipsoid, one of the principal indicatrix cross-sections is parallel to the symmetry plane *m*	$x_1 = x_5 \neq x_2 = x_8 \neq x_3 = x_7 \neq x_4 = x_6$
Tetrahexa-hedron {210}	*m*	biaxial ellipsoid, the principal axes are oblique to the face; the plane defined by the optical axes is parallel to the symmetry plane *m*	biaxial ellipsoid, one of the principal indicatrix cross-sections is parallel to the symmetry plane *m*	$x_1 = x_5 \neq x_2 = x_8 \neq x_3 = x_7 \neq x_4 = x_6$
Hexaocta-hedron {321}	1	biaxial ellipsoid, the orientation of the optical indicatrix is oblique	biaxial ellipsoid, the orientation of the optical indicatrix is oblique	$x_1 \neq x_2 \neq x_3 \neq x_4 \neq x_5 \neq x_6 \neq x_7 \neq x_8$

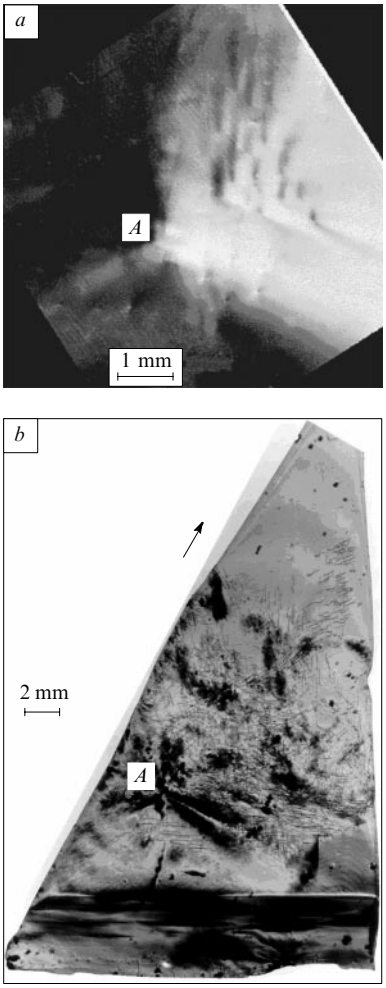


Figure 6. Subsector zoning in an alum $[K_{0.5}(NH_4)_{0.5}] \cdot Al(SO_4)_2 \cdot 12\,H_2O$ crystal. The cut is parallel to the (111) growth plane.[33]
(*a*) Anomalous birefringence around the top of a vicinal hillock (*A*); (*b*) an X-ray topogram of the cut, the arrow indicates the diffraction vector $\boldsymbol{g}$ direction for reflection 220.

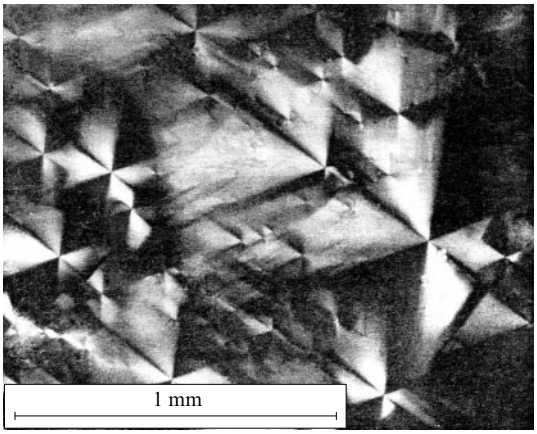


Figure 7. Optical subsector zoning in cuts of apatite crystals perpendicular to the [0001] crystallographic axis.[97]
The observed optical patterns correlate with the positions of vicinal hillock on the crystal face, although the correlation is ambiguous.

the resultant optical subsector zoning correlates with the vicinal face topography; and the symmetry of optical structures correspond to the symmetry of the face defined by the vicinal hillocks present on it.

Boundaries between different subsectors, *i.e.*, domains of a sector originated from different sides of a vicinal hillock, can be visualised in cuts parallel to the crystal growth direction. For instance, two vicinal hillocks formed by two dislocation bundles are clearly seen in the growth sector of the octahedral faces $(1\bar{1}1)$ for an alum crystal (Fig. 8). The crystal domains derived from different vicinal hillocks are characterised by differently oriented optical indicatrix, such that the interdomain boundaries can readily be seen in crossed polarisers (see Fig. 8).

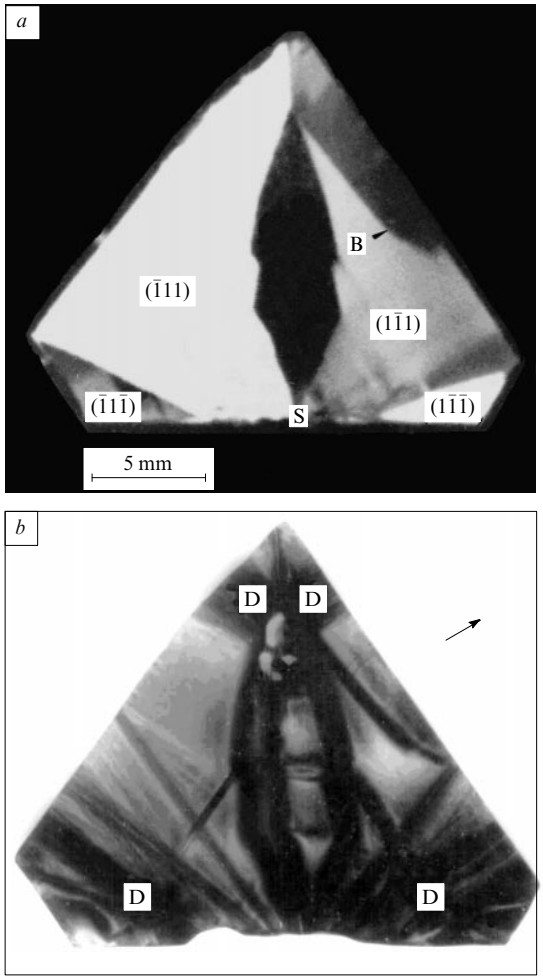


Figure 8. Subsector zoning in an alum $K(Al_{0.5}Cr_{0.5}) \cdot (SO_4)_2 \cdot 12\,H_2O$ crystal.[33]
(*a*) Anomalous birefringence in a plate, S is the seed crystal, B is the subsector zoning boundary between domains formed by growth steps from two vicinal hillocks; (*b*) X-ray topogram; the arrow indicates the diffraction vector $\boldsymbol{g}$ direction for reflection 333, D is a bundle of dislocations originated in the seed crystal S and a liquid inclusion.

3. The correlation between sector zoning and subsector zoning

Optical studies of crystals with the growth dissymmetrisation always reveal their prominent sectorial structure. The experimentally observed indicatrix fully agrees with the normal selectivity in the incorporation of isomorphous components. The optical subsector zoning resulted from the tangential selectivity in the incorporation of isomorphous components is often but not always the case. Typically, this is manifested weakly (minor variations in the systematic absences or a relatively small change in the birefringence). And it is rather surprising. Such crystals grow from mother liquors by the spiral dislocation mechanism, which implies that the faces grow through the movement of steps. Thus a

very distinct subsector zoning in the distribution of optical anomalies is anticipated in the majority of cases, which is not actually the case. This gives rise to an apparent contradiction: a crystal grows through the movement of steps, whereas the distribution of optical anomalies therein is better described by the normal mechanism of the crystal growth.

Several suggestions have been made to reconcile this controversy. According to one of them, the indicatrix strictly corresponding to the face symmetry, *i.e.*, to the case of the normal selectivity, is merely a net result of averaging of effects produced by numerous arbitrarily oriented steps forming this face. A modification of this hypothesis was elaborated by Gali.[148] Nevertheless, the growth of the vast majority of crystals proceed from a few (1–3) quite stable vicinal hillocks, which gives rise to a situation when rather large areas of a crystal are derived from identically oriented steps (see, for instance, Fig. 8), which contradicts the above mechanism. Another hypothesis assumes that the structural distortions occurring under the conditions of the tangential selectivity are close to those in the case of the normal selectivity, *i.e.*, the major energy difference between the sites results from their non-equivalence with respect to the crystal face. Additional non-equivalence due to the face step is negligible. In other words, although the tangential selectivity remains in effect, the ordering is apparently governed by the normal selectivity and the tangential selectivity effects can be revealed only in high-precision studies. We believe that this suggestion is very reasonable. According to another hypothesis, it is the diffusion relaxation that transforms the tangential selectivity ordering into the normal selectivity ordering.

4. Concentric zoning

Frequently, crystals grow under unsteady conditions, *i.e.*, temperature, growth rate, hydrodynamic regime, mother liquor composition can vary over time. Furthermore, the growing face morphology can undergo substantial changes in the course of the growth. All these factors affect the degree of ordering of isomorpous atoms and give rise to the concentric zoning in the distribution of optical parameters (which is often characterised by a very complex pattern). In this case, different extent of the dissymmetrisation under different growth conditions and at variable crystal composition acts as the key factor. The concentric zoning is observed in many crystals, in particular, in mixed alum crystals[29] and in garnets of the grossularite–andradite isomorphous series.[15] A special case of the continuous concentric zoning (also referred to as trend) not related to variations in the crystal composition and growth conditions, which has been reliably registered in mixed alum crystals,[149] is of particular interest. In that case, the birefringence and, consequently, the extent of the atomic ordering increased from the centre of the crystal towards its periphery first abruptly, then more smoothly finally approaching a plateau. It might be assumed that this pattern occurs due to the succession of relatively poor initial ordering (caused by the regeneration of the seed) in the growth under conditions providing a higher degree of the atomic ordering.

IV. Dissymmetrisation-induced changes in the crystal structure

As follows from the structural data gathered to date (see Table 1), the growth dissymmetrisation gives rise to insignificant changes in the topology of the crystal structure. This is due to the partial ordering of structural units (*i.e.*, atoms, ions, molecules or vacancies) in available crystallographic sites. The maximum degree of the growth ordering η of 0.84 (see below) was revealed in vesuvianite $Ca_{19}(Mg,Fe,Al)_{13}\cdot Si_{18}O_{68}(O,OH,F)_{10}$ crystals.

Typically, the degree of distortion of unit cell parameters is small, but it continuously increases with perfection of the ordering in the distribution of structural units. This trend can be illustrated by a linear increase in the monoclinic angle β in initially cubic structures of garnets $Ca_3(Al,Fe,Cr)_2(SiO_4)_3$ and sodium chlorate bromate $Na(ClO_3,BrO_3)$ with an increase in the difference between the occupancies of initially equivalent sites (*i.e.*, Al and ClO_3^- occupancies x_1 and x_2 in the two available trivalent cationic and anionic sites for the former and latter compounds, respectively, Fig. 9).

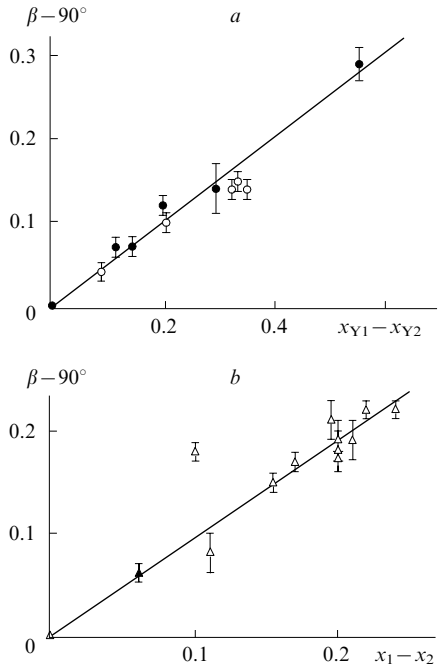


Figure 9. Monoclinic angle as a function of the difference in site occupancies.
(*a*) Garnets of the grossularite–andradite (plain symbols, data taken from Refs 6, 14–16) and grossularite–uvarovite (shaded symbols, data taken from Ref. 17) isomorphous series, the growth sector {110}; (*b*) sodium chlorate bromate solid solutions, the growth sector {100}; plain symbols are from Ref. 27, two superimposed shaded symbols are from Ref. 25.

Typically, the atomic ordering does not lead to the appearance of a superstructure. However, there are some exceptions to this rule. In particular, a superstructure due to the ordering of calcium and magnesium atoms was revealed in calcite and dolomite crystals using high-resolution transmission electron microscopy.[103] Unfortunately, the growth origin of the superstructure has not been confirmed so far.

According to studies of a series of solid solutions belonging to one structural type [*e.g.*, garnets[6,14–17] and minerals of the pollucite–analcime series $Cs_xNa_{1-x}AlSi_2O_6\cdot(1-x)\,H_2O$ (Refs 22–25)], a variety of solid solutions with different symmetries and occupancies of crystallographic sites can be derived from the same isomorphous series owing to the dissymmetrisation. Frequently, the normal selectivity in the distribution of the occupancies is suggested based on a preliminary analysis, whereas a more thorough analysis yields a lower space group corresponding to the tangential selectivity (see above).

In particular, the dissymmetrisation of garnets of the grossularite–andradite and grossularite–uvarovite isomorphous series (the growth sector {110}, ideal space group $Ia\bar{3}d$) should give rise to the splitting of one octahedral cationic site Y to two sites, Y1 and Y2, with the respective symmetry lowering to orthorhombic, in the case of the normal selectivity in the incorporation of trivalent cations. Under the conditions of the tangential selectivity, each of the two sites is further split into four ones (Y1*i*, Y2*i*, $i = 1-4$), which corresponds to the triclinic symmetry. X-ray diffraction studies of eleven garnet crystals of these isomorphous series manifesting optical anomalies[6,14–17] showed that the symmetry of seven crystals lowered to triclinic, whereas the symmetry of remaining four crystals was orthorhombic. Moreover, the triclinic crystals were distinctly pseudoorthorhombic,

i.e., it was possible to subdivide the eight octahedral cationic sites therein into two tetrads of sites in such a way that differences in the site occupancies within a tetrad were significantly less pronounced than those between the tetrads. Formally, this pseudoorthorhombicity can be quantified with a 'triclinicity factor'

$$\xi = \frac{\max\left(|x_{1i} - x_{1j}|, |x_{2i} - x_{2j}|\right)}{|x_1 - x_2|}, \quad i, j = 1-4,$$

where x_1 and x_2 are the occupancies of the sites Y1 and Y2, respectively; x_{1i} and x_{2i} are the occupancies of the sites Y1*i* and Y2*i*, respectively.

Based on the orthorhombic or pseudoorthorhombic lattice, the degree of the cation ordering in the two sites can be calculated as

$$\eta = \frac{x_1 - x_2}{1 - |1 - x_1 - x_2|}.$$

A comparative analysis of the experimental data on all eleven crystals indicated that both parameters vary over wide ranges: ξ is ranged between 0.045 and 0.74, whereas η varies from 0.065 to 0.79.[16]

Another example considers the dissymmetrisation of the growth sectors {100} in sodium chlorate bromate $Na(ClO_3, BrO_3)$ crystals (ideal space group $P2_13$), where the normal selectivity leads to the splitting of a single site statistically occupied by chlorine and bromine atoms into two ones, which is accompanied by a decrease in the symmetry to monoclinic (space group $P2_1$). Under the conditions of the tangential selectivity, all four sites appear differently occupied, which corresponds to the triclinic symmetry (space group $P1$). Such a symmetry lowering to monoclinic or triclinic (pseudomonoclinic) was indeed observed in thirteen crystals studied using X-ray diffraction.[26–28] As in the case of garnets discussed above, the ordering degree and the triclinicity factor varied in a wide range from one crystal to another.

The correlation between ordering of atoms in different structural sites is yet another specific feature of the growth dissymmetrisation. It is driven by the requirement to keep the local charge balance. This effect is very distinctly manifested in analcimes[22] and pollucite–analcime solid solutions $CsAlSi_2O_6$ (pollucite)–$NaAlSi_2O_6 \cdot H_2O$ (analcime).[24,25] In the case of analcimes, the decrease in the symmetry from cubic (space group $Ia\bar{3}d$) to tetragonal (space group $I4_1/acd$) or orthorhombic (space group *Ibca*) is caused by the ordering of the aluminium and silicon cations in the tetrahedral sites and of the sodium cations and vacancies in the octahedral sites. A linear correlation between the fraction of the aluminium in a tetrahedral site and the fraction of sodium in the closest octahedral site was established (Fig. 10). The symmetry of pollucite–analcime solid solutions decreases to orthorhombic (space group $I2_12_12_1$) due to the same reasons and, in addition, due to the partial ordering in the distribution of the caesium cations and water molecules in channels of the Al/Si framework. Respectively, there is an apparent trend towards a linear correlation between the aluminium occupancy in a tetrahedral site and the content of monovalent cations (Cs + Na) in the closest positions.[25]

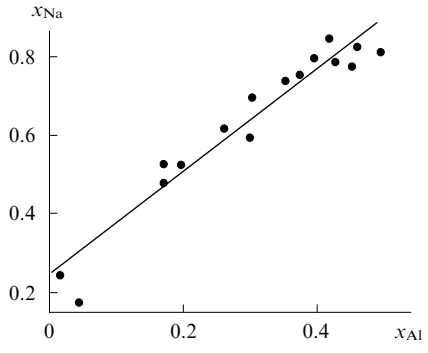


Figure 10. Sodium occupancy x_{Na} as a function of Al occupancy in the nearest tetrahedral site x_{Al} for birefringent analcime crystals.[22]

The simultaneous ordering of cations in sites X and Y can also take place in the crystal structures of naturally occurring garnets $X_3Y_2(SiO_4)_3$ [X = Ca, Fe(II), Mg, Mn(II); Y = Al, Fe(III)].[8] The kinetic ordering in ugrandite garnets $Ca_3Y_2(SiO_4)_3$ is well known (see above); however, no dissymmetrisation has been observed in related pyralspite garnets $X_3Al_2(SiO_4)_3$.[150–153] This implies that the ordering in the sites X of the garnet crystals occurs simultaneously with the ordering in the sites Y. The isomorpous isovalent substitution in the sites X and Y does not violate the charge balance, which assumes that the correlation in this case is driven by the necessity to compensate for local structural stresses emerging due to different sizes of the atoms subject to ordering.[17]

The kinetic ordering-induced dissymmetrisation of a crystal structure, which typically retains the structural type, is usually manifested in significant mutually correlated deformations of different coordination polyhedra. For instance, the ordering in the distribution of the Al and Cr/Fe cations in the octahedral sites Y of the crystal structures of ugrandite garnets gives rise not only to substantial changes in the Y–O and O–O bond lengths (Fig. 11) but also to variations in the O–Si–O bond angles in the SiO_4 tetrahedra that link the octahedra through shared vertices, which results in the respective tilt of the tetrahedra (Fig. 12).[6,17]

Dissymmetrisation-induced changes in the crystal structures can be efficiently described with cluster models.[17,24,25] For

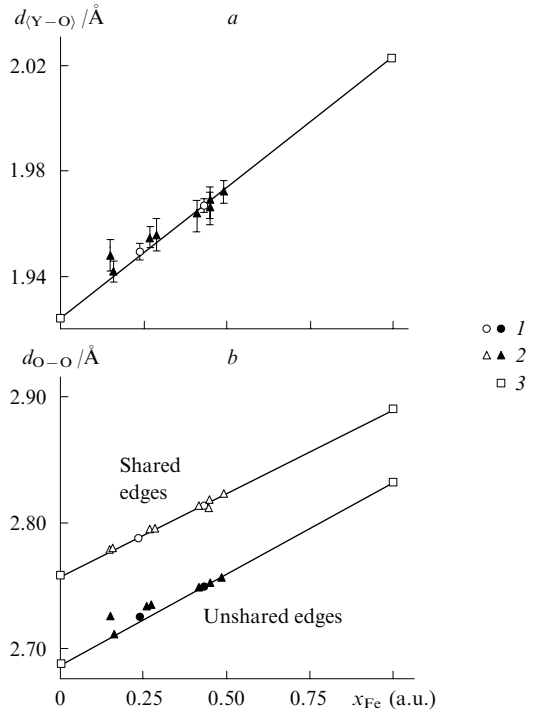


Figure 11. Change in the size of the YO_6 octahedra as a function of the iron occupancy in the site Y for a garnet $Ca_3(Al_{0.68}Fe_{0.32})_2(SiO_4)_3$ crystal (the sample Munam from Ref. 6).
(*a*) The Y–O bond lengths, (*b*) the O–O edge lengths (the shared and isolated edges are plotted as plain and shaded symbols, respectively). The crystal structure was refined in the orthorhombic space group *Fddd* (*1*) and the triclinic space group $I\bar{1}$ (*2*), the straight lines are drawn through the data points corresponding to the end members of the series (*3*).

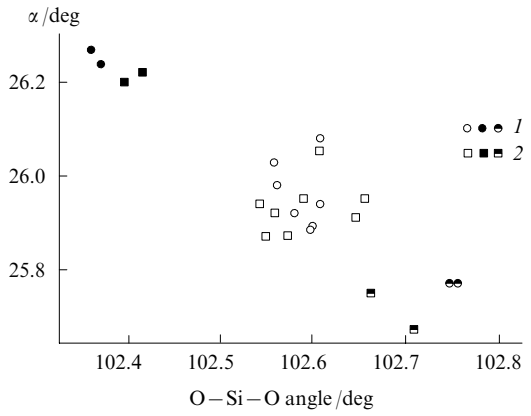


Figure 12. The tilting angle of the SiO_4 tetrahedra α as a function of the O–Si–O angle formed by the O–O edge shared with the CaO_8 polyhedron for two low-symmetry garnet $Ca_3(Al,Cr)_2(SiO_4)_3$ samples (symbols *1* and *2*).[17]
The tetrahedral edges that link two neighbouring octahedra preferably occupied by Cr (both octahedra), Al (both octaheda) and Cr (the first octahedron) and Al (the second octahedron) are marked with the shaded, half-shaded and plain symbols, respectively.

instance, in the structure of low-symmetry ugrandite garnets $Ca_3Y_2(SiO_4)_3$ (Y = Al, Cr, Fe), chromium/iron-rich and chromium/iron-poor CaY_4O_{24} clusters can be distinguished, which alternate along the [010] axis (in the pseudocubic setting, see Table 10) and are linked with each other with SiO_4 tetrahedra (Fig. 13).[17] The clusters include octahedra of the same type or those belonging to one tetrad in orthorhombic and triclinic garnets, respectively.

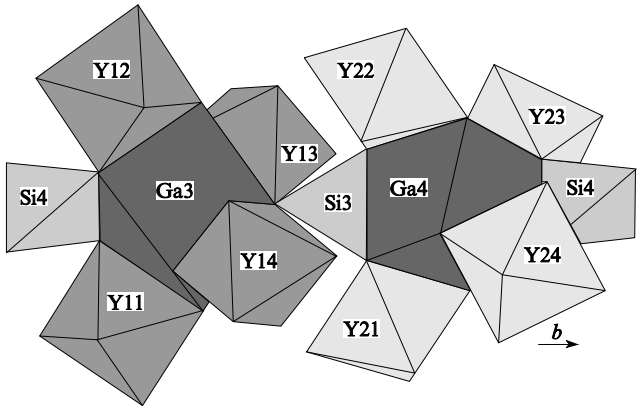


Figure 13. Cr-rich and Cr-poor CaY_4O_{24} clusters alternating along the [010] crystallographic axis (in the pseudocubic setting) in the crystal structure of low-symmetry garnet $Ca_3(Al,Cr)_2(SiO_4)_3$ crystals.[17]

V. The metastability of the kinetic ordering

The ordered state, which is equilibrium with respect to the crystal surface, becomes metastable upon transition to the bulk. This initiates the process of the diffusion equilibration of the site occupancies. As a rule, this process is characterised by a negligibly low rate at room temperature due to the very slow diffusion in solids. However, such a diffusion relaxation in the bulk of the crystal decreasing the dissymmetrisation degree should proceed much faster upon the high-temperature annealing ($T > 0.8\,T_{mp}$). This effect was indeed observed for a number of crystalline compounds, including quartz,[78,79] brookite TiO_2,[111] topaz,[69] analcime,[154] ralstonite $Na_xMg_xAl_{2-x}(OH,F)_6 \cdot H_2O$,[88] sodium chlorate bromate,[26,27] garnets of the grossularite–andradite isomorphous series,[6,8,15,155] synthetic garnets $(Y_{0.53}Nd_{0.47})_3.Ga_5O_{12}$,[20] alum,[156] lead strontium nitrate,[36] *etc*. It is of note that the term 'high-temperature annealing' is ambiguous. Alum solid solutions $(K,NH_4)Al(SO_4)_2 \cdot 12\,H_2O$ ($T_{mp} \approx 90$ °C) undergo the annealing already at room temperature, which gives rise to the spontaneous attenuation of the birefringence upon prolonged storage. The initial crystal structures of a garnet and sodium chlorate bromate crystals manifesting the anomalous birefringence were refined and compared to those after the complete relief of the optical anomalies by a high-temperature treatment.[8,26,27] It was demonstrated that the annealing results in the equilibration of the site occupancies and the disappearance of the ordering (as well as of the birefringence).

Let us consider a crystal containing two types of atoms occupying two structural sites in an ordered way. Let us denote the sites with a subscript $i = 1, 2$; the mole fractions of one of the components in the first and second sites are x_1 and x_2, respectively. In overall, any type 1 site has n_{1-1} and n_{1-2} closest neighbours of the types 1 and 2, respectively. By considering the diffusion as a random walk of an atom and assuming only jumps between the adjacent sites, one can write the kinetic equation, which statistically characterises the time changes in the concentration of this component in the site 1 (the result will not change if the site 2 is considered), as follows

$$\frac{dx_1}{dt} = \frac{n_{1-1}P_E x_1 + n_{1-2}P_E x_2}{n_{1-1} + n_{1-2}} - P_E x_1 = \tag{1}$$

$$= \frac{n_{1-2}}{n_{1-1} + n_{1-2}} P_E(x_2 - x_1) = n^* P_E(x_2 - x_1).$$

Here, t is time, P_E is the probability of an atomic jump to a neighbouring (vacant) site, $n^* = n_{1-2}/(n_{1-1} + n_{1-2})$. The solution of this equation is given by

$$\frac{x_2 - x_1}{x_{20} - x_{10}} = \exp(-2n^* P_E t) = \exp\left(-\frac{2n^* Dt}{h^2}\right), \tag{2}$$

where $(x_2 - x_1)$ and $(x_{20} - x_{10})$ are the differences in the site occupancies for the crystal before and after the annealing for a duration t, h is the distance between the neighbouring sites i, D is the self-diffusion coefficient, $D = h^2 P_E$ [strictly speaking, the self-diffusion coefficients should be different for each type of atoms, therefore, an effective mean value is placed in Eqn (2)]. Let us assume that the birefringence Δn (or another appropriate quantitative criterion for the distortion of the optical indicatrix) is directly proportional to the differences in the concentrations of one type of atoms in different sites. This assumption is reasonable, which is supported by simulations of the optical indicatrix based on the crystal structure data [15] (Fig. 14). The transition of the crystal from the birefringent to the isotropic state can be regarded as a quasichemical reaction. The conversion level (ξ) can then be written as

$$\xi = \frac{\Delta n}{\Delta n_0} = \exp\left(-\frac{2n^* Dt}{h^2}\right) = \exp(-kt). \tag{3}$$

This implies that the relief of optical anomalies should obey the first-order reaction kinetics and thus the birefringence should exponentially attenuate with the annealing time. The reaction rate constant k includes the self-diffusion coefficient of atoms, which in turn exponentially depends on temperature

$$D = D_0 \exp\left(-\frac{E_d}{RT}\right). \tag{4}$$

(E_d is the activation energy of self-diffusion).

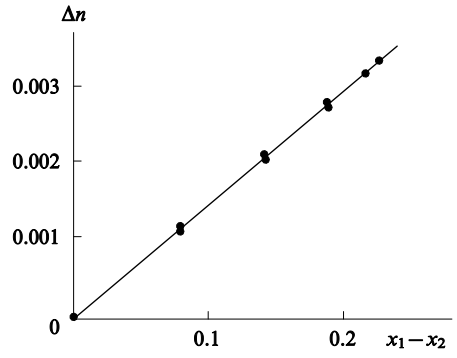


Figure 14. Anomalous birefringence as a function of the difference in the iron occupancies between the two octahedral cationic sites Y_1 and Y_2 for garnets of the grossularite–andradite isomorphous series (calculated in the orthorhombic space group *Fddd*), adapted from Ref. 15.

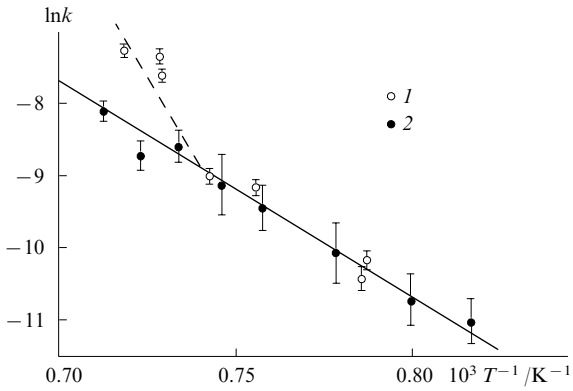


Figure 16. Temperature dependences of the rates of anomalous birefringence attenuation for two garnet crystals (the data points *1* and *2*).[15]

This implies that the rate of the relief of optical anomalies exponentially increases with an increase in the annealing temperature.

These theoretical conclusions agree well with the available experimental data. The relaxation kinetics upon annealing for crystals manifesting the growth ordering of atoms was elucidated for quartz,[78,79] two isomorphous alum series, *viz*., $(K,NH_4)Al(SO_4)_2 \cdot 12\,H_2O$ and $K(Al,Cr)(SO_4)_2 \cdot 12\,H_2O$,[156] garnets of the grossularite–andradite series $Ca_3(Al_{0.9-0.5}Fe_{0.1-0.5})_2 \cdot (SiO_4)_3$ (Ref. 15) and lead strontium nitrate solid solutions.[36]

The case of garnets is considered in more detail below. The kinetics of the attenuation of the birefringence upon annealing was elucidated for two crystals from the Mali deposit. It was found that different parts of the same crystal were characterised by different birefringence attenuation rate constants k. In particular, for one of the crystals, the transformation rate was 3.3 times higher for its outer part, which is characterised by an increased content of water, titanium and defects (dislocations), than in a more perfect central part. And this is logical since the self-diffusion accelerates in areas with a higher defect concentration, since its mechanism involves vacancies. The experimental kinetic points form straight lines in the Arrhenius plot (Fig. 15). The lines are characterised by identical slopes within the experimental accuracy, and the differences between them are exclusively due to the preexponential factors. Similar trends are characteristic of different growth sectors in alum crystals. According to a set of experimental data on two garnet crystals (Fig. 16), the activation energy of transition from the birefringent to the isotropic state is 249 ± 12 kJ mol^{-1} in a temperature range from 950 °C to 1090 °C. Data points measured above 1090 °C for one of the crystals deviate strongly from the common trend giving rise to a kink in the plot, which is manifested in the experiment as an abrupt acceleration of the birefringence attenuation at a temperature about 1090 °C (see Fig. 16). This can be rationalised assuming an alteration of the diffusion mechanism, which results in a strong acceleration of the anomalous birefringence attenuation. Presumably, the diffusion mechanism is controlled by the concentration of preexisting vacancies (due to admixtures or linear defects) at a sufficiently low temperature, whereas thermally generated vacancies start to play a key role at high temperature.[157,158] In addition to the observed trends in the activation energy of thermal curing of optical anomalies in garnets as a function of temperature, this suggestion explains why it is constant in different crystals or in different zones and sectors of one crystal despite strong variations in the preexponential factors that depend on the vacancy concentration. Similar observations were made for alum crystals[156] and lead strontium nitrate solid solutions.[36]

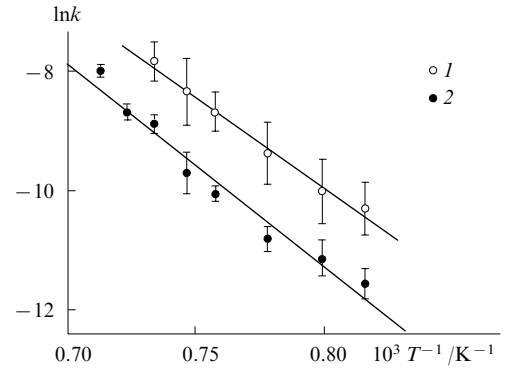


Figure 15. Temperature dependences of the rates of anomalous birefringence attenuation for the central part (*1*) and periphery (*2*) of a garnet $Ca_3(Al_{0.5-0.7}Fe_{0.5-0.3})_2(SiO_4)_3$ crystal.[15]

Unfortunately, accurate values of the self-diffusion coefficients of trivalent cations in grandites are unknown. On the other hand, extensive information on the diffusion coefficients of bivalent cations in pyralspites[159–162] (see also references cited in Ref. 162) is available. The activation energies of diffusion for bivalent cations range from 155 to 290 kJ mol^{-1}. These values agree well with the experimental activation energies of birefringence attenuation upon annealing, which strongly supports the diffusion nature of the process.

VI. The kinetic ordering and the atomic structures of growing faces

The close relation of the dissymmetrisation ordering to the surface atomic structure of a growing crystal (neglecting possible surface reconstruction or relaxation) can be considered as an argument in favour of its growth origin. A careful analysis of sites equivalent in the bulk of a crystal reveals their geometrical differences with respect to faces and growth steps on faces, which is the main driving force for the atomic ordering in the course of the crystal growth. Such an approach has been demonstrated above as applied to the analysis of site symmetries. In that case, only the possibility of the manifestation of differences was stressed, although a direct analysis of the surface structures makes it possible to elucidate these differences in more detail. The surface structures were determined for a number of compounds, including quartz SiO_2,[75,79] cordierite $Mg_2Al_3(AlSi_5O_{18})$,[43] chabazite $Ca_2Al_4 \cdot Si_8O_{24} \cdot 13\,H_2O$,[108] topaz $Al_2SiO_4(OH,F)_2$,[69] stilbite $Na_2Ca_4Al_{10}Si_{26}O_{72} \cdot 34\,H_2O$,[116] adularia $KAlSi_3O_8$,[63] yugawaralite $CaAl_2Si_6O_{16} \cdot 4\,H_2O$,[73] garnets $Ca_3(Al,Fe)_2(SiO_4)_3$,[7,14] brew-

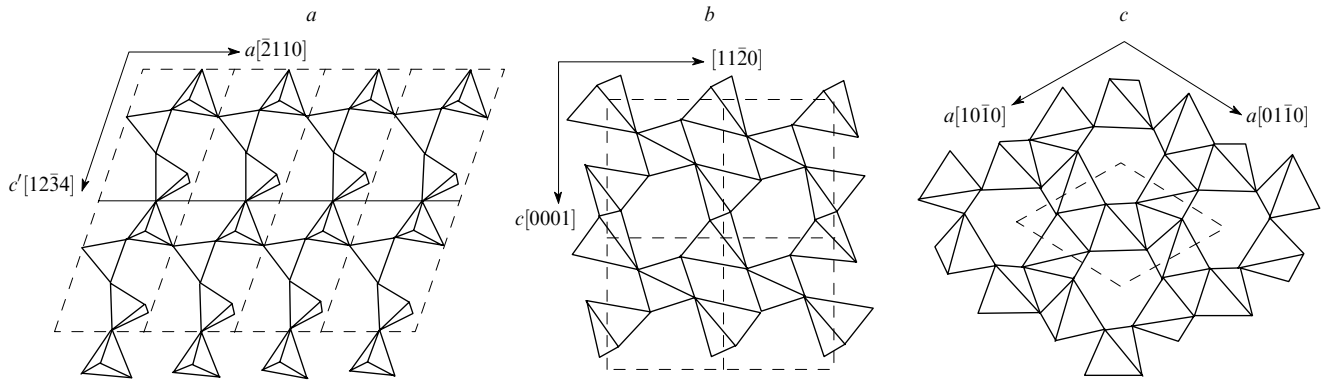


Figure 17. Projections of the crystal structure of α-quartz onto the $\{01\bar{1}1\}$ (*a*), $\{\bar{1}\bar{1}20\}$ (*b*) and $\{0001\}$ (*c*) crystallographic planes.[79]

sterite $(Sr,Ba)_2Al_2Si_{12}O_{32}\cdot 10\,H_2O$ (Ref. 67), *etc*. Below, the correlation between ordering in quartz and the structure of its faces is considered in more detail (*cf*. Ref. 79). Geometrical differences in the arrangement of the SiO_4 tetrahedra with respect to the crystal growth front can be analysed using projections of the crystal structure of quartz onto planes corresponding to faces belonging to possible regular forms of the crystal, *i.e*., rhombohedron, prism and pinacoid (Fig. 17). There are three possible arrangements of the silica tetrahedra relative to the rhombohedral faces (in the respective growth sectors, the hole concentrations are different for all three possible oxygen sites). Relative to the prismatic faces, there are two non-equivalent orientations of the silica tetrahedra (two out of three oxygen sites are characterised by identical hole occupancies). Finally, all tetrahedra are oriented identically with respect to the pinacoidal faces (*i.e*., all three oxygen sites are equally occupied by holes). Therefore, the ratios between the site occupancies correlate with the geometrical orientation of different SiO_4 tetrahedra with respect to the growth front, which explains how the crystal face symmetry determines the crystal symmetry resulted from the growth ordering. The atomic structure of a face provides the geometrical non-equivalence of the sites according to the face symmetry, which gives rise to the dissymmetrisation.

In a similar way, tight interrelation between the atomic structure of faces and resultant distribution of site occupancies with isomorphous atoms was established for garnets of the grossularite–andradite isomorphous series[14] and sodium chlorate bromate.[28]

VII. The diffusion relaxation

The ordering of isomorphous components emerging in the course of the crystal growth in steps or on a surface layer tends to relax directly during the growth via the diffusion-driven intersite exchange. The mechanism of the diffusion relaxation was considered by Chernov *et al*.,[122] as applied to the non-equilibrium incorporation of isomorphous admixtures. We modified this mechanism to extend it to the kinetic ordering of atoms in the crystal structure.

Let us consider the growth of a mixed crystal, where isomorphous atoms can be ordered in several sites that are equivalent in the bulk but different with respect to steps and faces. In such a case, the occupancy of the sites by isomorphous atoms can be described with the equilibrium distribution coefficients (see Section VIII.1), which are different for steps, faces and the bulk of the crystal due to different geometrical environments. When atoms are incorporated in steps, the non-equivalent sites get differently occupied by isomorphous atoms in agreement with the actual growth medium composition and growth conditions, *i.e*., an atomic distribution corresponding to the tangential selectivity is realised. As soon as the step appears completed thus transforming into a surface layer, the preformed atomic distribution becomes non-equilibrium, since the geometrical environment of the sites has changed. Thus this state tends to transform into the state that is equilibrium for a surface layer, *i.e*., the one corresponding to the normal selectivity, by means of the diffusion redistribution of atoms. Such a diffusion redistribution proceeds until the layer is completely covered with the next one thus entering the bulk of the crystal. All the sites appear equivalent in the bulk of the crystal and thus the diffusion redistribution will tend to equilibrate the site occupancies completely. However, this process can proceed efficiently only at a high temperature (*i.e*., upon annealing, see Section V).

Let us consider a crystal surface layer formed by the movement of a growth step, which is non-equilibrium with respect to the solution. The rate of atomic exchange between any site on the crystal surface and the solution is determined by the probability of the detachment of an atom from the surface layer (P_d). This process is accompanied by a change in the concentration x_i of an element in the site i from a value x_{si} corresponding to the equilibrium between the step and the solution to a value x_{fi} required by the equilibrium between the face and the solution. The rate of this change can be written as

$$\frac{dx_i}{dt} = (x_{fi} - x_{si})P_d\,. \tag{5}$$

The probability of the detachment of an atom from the surface layer is given by

$$P_d = \frac{D_s}{h^2}\,,$$

where D_s is the diffusion coefficient for the transition of an atom from the surface layer to the growth medium, h is the height of an elementary step. By solving this equation with a boundary condition $x_i(0) = x_{si}$, one gets

$$\frac{x_{fi} - x_i}{x_{fi} - x_{si}} = \exp(-\tau_{ml}P_d). \tag{6}$$

Here, $\tau_{ml} = h/V$ is the time period required to cover the surface layer with a new one, *i.e*., the monolayer formation time; V is the normal crystal growth rate. The resultant occupancies are then as follows

$$x_i = x_{fi} + (x_{si} - x_{fi})\exp\left(-\frac{D_s}{Vh}\right). \tag{7}$$

To a first approximation, the diffusion coefficient is given by the following equation

$$D_s = \nu h^2 \exp\left(-\frac{E_s}{RT}\right), \tag{8}$$

where $\nu = 10^{12}$ s^{-1} is the frequency of atomic vibrations, E_s is the activation energy of diffusion of atoms from the crystal surface to the mother liquor.

For a transition from a lower-symmetry to a higher-symmetry phase, the left-hand side of Eqn (6) represents the degree of completion of the transition [*i.e.*, the order parameter defined by the exponential term in the expression (7)]

$$\eta = \exp\left(-\frac{D_s}{Vh}\right).$$

If this exponential term is close to unity (*i.e.*, the diffusion rate is low as compared to the crystal growth rate), $x_i = x_{si}$ and no diffusion redistribution of occupancies occurs, then a state corresponding to the initial ordering in the step (the tangential selectivity case) is preserved in the bulk of the crystal. To the contrary, if the exponential term is close to zero (the diffusion rate is high as compared to the crystal growth rate), then $x_i = x_{fi}$. In this case, the diffusion redistribution effectively proceeds until completion such that a new state corresponding to the surface layer ordering (the normal selectivity case) enters the bulk of the crystal.

Unfortunately, no information on E_s is available, which hinders quantitative estimates based on this mechanism. Nevertheless, let us assume that the activation energy of detachment of an atom from the crystal surface layer E_s is higher than the activation energy of crystal dissolution E_{ds} and lower than the activation energy of bulk self-diffusion E_d. This assumption is based on the following arguments. The detachment of an atom from step kinks (which is the main process responsible for the crystal dissolution) requires several bonds to be broken. But this number is certainly less than that required to remove an atom from the surface layer and, especially, from the bulk. Due to the fact that E_{ds} and E_d can be realistically estimated, at least upper and lower estimates of E_s can be obtained to a good approximation. Two examples are given below.

The dissymmetrisation in garnets of the grossularite–andradite isomorphous series gives rise to the decrease in the initial cubic symmetry to either orthorhombic space group *Fddd* (due to the ordering of cations in two sites, which corresponds to the normal selectivity case) or to triclinic space group $I\bar{1}$ (due to the ordering of cations in eight sites, which corresponds to the tangential selectivity case). Naturally occurring garnet crystals differ drastically in the normal growth rates: from one cm per 10 million years to one cm per year; a detailed analysis of these data can be found elsewhere.[163] For further calculations, let us take the maximum value (10^{-9} m s^{-1} or 3.1 cm per year), which is most reasonable, in our opinion. The detachment of a cation from an octahedral site (Al, Fe) of the surface layer in a garnet crystal requires the breakage of three to four bonds, depending on the orientation of the respective octahedron. Meanwhile, only two bonds have to be broken for the detachment of an atom from a step kink. Thus, to a first approximation, one may assume that $E_s \approx 1.75\,E_{ds}$. To our knowledge, no experimental measurements of E_{ds} for grandites have been reported. However, this value can be estimated based on the activation energies of growth and dissolution for other crystals grown under comparable conditions (in particular, hydrothermal ones). According to Dem'yanets (personal communication) and Kuznetsov,[164] the activation energies of crystal growth E_g lie within a range of 33–92 kJ mol^{-1} for a number of oxides and silicates [*e.g.*, quartz, cancrinite $Na_6Ca_2(AlSiO_4)_6(CO_3)_2$, sodalite $Na_4Al_3Si_3O_{12}(Cl)$, Al_2O_3, ZnO, TeO_2] except for corundum (for which it amounts to 130 kJ mol^{-1} for some of the regular forms). Typically, the specific heat of crystallisation ΔH does not exceed 20 kJ mol^{-1}, therefore

$$E_{ds} = E_g + \Delta H = 53-112 \text{ kJ mol}^{-1}.$$

According to results by Lasaga,[157] the activation energy of dissolution E_{ds} is 37–75 kJ mol^{-1} for diopside $CaMgSi_2O_6$, enstatite $Mg_2Si_2O_6$, augite $(Ca,Na)(Mg,Fe,Al)(Si,Al)_2O_6$, forsterite Mg_2SiO_4 and quartz (150 kJ mol^{-1} was given as the upper estimate for diopside). The published data on the activation energy of dissolution for almandine crystals $Fe_3Al_2(SiO_4)_3$ (E_{ds} = 46–54 kJ mol^{-1}, see Ref. 165) and on the crystallisation kinetics of pyralspites $(Fe,Mg,Mn,Ca)_3Al_2(SiO_4)_3$ (E_g = 50 kJ mol^{-1}, see Ref. 163) also fall into the above ranges. Therefore, the upper estimate of the activation energy of dissolution for grandite $Ca_3(Al,Fe)_2(SiO_4)_3$ crystals is 110 kJ mol^{-1}, whereas that of E_s is 192 kJ mol^{-1}. The most probable mean values are E_{ds} = 60 kJ mol^{-1} and E_s = 105 kJ mol^{-1}.

According to experimental data on the annealing of grandites, the activation energy of cation self-diffusion is 249 kJ mol^{-1} (see Section V). A jump of a cation from one octahedral site into another one requires six bonds to be broken, therefore

$$E_s \approx 0.58\,E_d = 145 \text{ kJ mol}^{-1},$$

which agrees well with the previous estimate.

Calculations according to the Eqn (7) indicate that either triclinic or orthorhombic phase enters the bulk of the crystals, depending on the crystallisation temperature and the activation energy of detachment of a cation from an octahedral site (Fig. 18*a*). For a constant E_s, the choice of the resultant modification depends on the crystallisation temperature. Typically, the crystallisation temperature lies in a range of 200–700 °C, thus the orthorhombic phase should form exclusively if the activation energy is equal or lower than 100 kJ mol^{-1} (which is of low probability). On the other hand, the exclusive formation of the

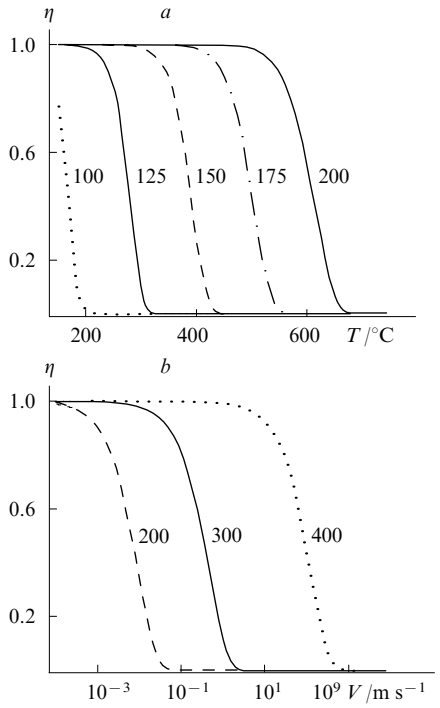


Figure 18. Ordering parameter as a function of the crystallisation temperature and activation energy of the detachment of an atom (*a*) and on the growth rate (*b*) in a garnet crystal (the values $\eta = 1$ and $\eta = 0$ correspond to the most ordered triclinic and orthorhombic structures, respectively). Adapted from Ref. 16.
(*a*): Numbers at the curves correspond to the activation energies in kJ mol^{-1}, the growth rate is 10^{-9} m s^{-1}; (*b*): numbers at the curves correspond to the crystallisation temperature in °C, the activation energy is 125 kJ mol^{-1}.

triclinic phase is expected for $E_s > 230$ kJ mol^{-1} (which is of very low probability). For intermediate values of E_s (which is apparently the most realistic estimate), the preferable crystal structure (symmetry) is governed by the crystallisation temperature. This explains the fact that both orthorhombic and triclinic garnets occur in nature. The value of the order parameter η is also affected by the crystallisation rate (Fig. 18 *b*), which acts in this case as the control parameter of the kinetic phase transition.

The dissymmetrisation of sodium chlorate bromate crystals for the growth sector of the cubic faces gives rise to a symmetry decrease from cubic to monoclinic or triclinic (which correspond to the cases of the normal and tangential selectivity in the incorporation of isomorphous cations, respectively). The crystals are usually grown at a low temperature from aqueous solutions. Thus typical growth rates, the specific heat of crystallisation and the activation energy of crystal growth are reliably established.[166–169] According to calculations, the activation energy of dissolution varies from 35 to 40 kJ mol^{-1}. Three to four bonds have to be broken to remove a $HalO_3^-$ anion from a step kink. Meanwhile, the detachment of an anion from the surface layer requires the breakage of five bonds. Taking this into account, one gets

$$E_s \approx 1.43\, E_{ds} = 50-57 \text{ kJ mol}^{-1}.$$

A calculation based on this estimate together with typical growth rates (*viz.*, $0.1-5\times10^{-8}$ m s^{-1}) predicts either monoclinic modification or an intermediate structure transient to the most ordered triclinic modification, *i.e.*, indicates a border zone between the two structures, which completely agrees with the experimental observations.

VIII. Control factors of the kinetic ordering

1. Solid solution composition

Let us consider the degree of the kinetic ordering of atoms along isomorphous series as a function of the ratio of well miscible components (*e.g.*, ideal isomorphism in garnets, alum, *etc.*). We assume that two components, A and B, of a completely miscible solid solution undergo ordering in two non-equivalent subsystems of sites, which initially belonged to the same regular system of points. Let us denote the subsystems with a subscript $i = 1, 2$. Presumably, each of the subsystems behaves independently as regards the crystal growth and is characterised by its own distribution coefficient K_i with respect to the solution (crystallisation medium). The distribution coefficient K_i is used in the following equation (for a definition of K_i, see, for instance, Ref. 170)

$$\frac{x_i}{1-x_i} = K_i \frac{y}{1-y}. \tag{9}$$

Here, x_i is the mole fraction of one of the components (*viz.*, B) in the site i of the crystal and y is the respective mole fraction of the same component in the solute. The distribution coefficients defined in this way are independent of the ratio of the components A and B both in the crystal and the solution assuming that the solid solution insignificantly deviates from the ideal solution. The ratio of the left-hand sides of Eqn (9) for different subsystems i yield the so-called intersite distribution coefficient

$$K = \frac{K_2}{K_1} = \frac{1-x_1}{x_1}\frac{x_2}{1-x_2}. \tag{10}$$

In order to determine the difference between the incorporation of the component B in the different subsystems, one should express the site occupancy by the component B through its average content in the crystal

$$x = \frac{n_1x_1 + n_2x_2}{n_1 + n_2}$$

and the difference in the occupancies is then equal to

$$\delta = \frac{x_1 - x_2}{n_1 + n_2} > 0,$$

where n_i is the total number of sites in the subsystem,

$$x_1 = x + n_2\delta, \qquad x_2 = x - n_1\delta. \tag{11}$$

The sum

$$n_1 + n_2 = n$$

is referred to as the multiplicity of this regular system of points in the parent high-symmetry space group. Within the notation scheme used, $x_1 > x_2$ and $0 < K < 1$. After substitution of expression (11) into Eqn (10), an equation quadratic on δ is yielded. This equation has two solutions, only one of which has physical meaning

$$x_1 - x_2 = \frac{n_1 + n_2}{2n_1n_2}\left\{x(n_2 - n_1) + \frac{Kn_2 + n_1}{1-K} - \sqrt{\left[x(n_2 - n_1) + \frac{Kn_2 + n_1}{1-K}\right]^2 - 4x(1-x)n_1n_2}\right\}. \tag{12}$$

If $n_1 = n_2$, the resultant function is symmetric with respect to $x = 0.5$. If K deviates significantly from 1, the function can be represented as two virtually linear segments intersecting at $x = 0.5$. If K is close to 1 (the degree of ordering is low), the resultant expression is reduced to

$$x_1 - x_2 \approx \frac{2(1-K)}{1+K}x(1-x), \tag{13}$$

which implies that the difference of site occupancies depends parabolically on the crystal composition. The deviation of the approximate expression (13) from the accurate one (12) reaches the maximum for the middle of the isomorphous series and depends on the distribution coefficient: the difference rapidly decreases as K approaches unity (which means that the difference between the site occupancies becomes small). In particular, the difference is 40% for $K = 0.01$, it decreases to 21% for $K = 0.1$ and further to 13% for $K = 0.2$ becoming negligibly small ($< 5\%$) already for $K = 0.4$. If $n_1 \neq n_2$, the maximum of $(x_1 - x_2)$ shifts towards the component B, provided that $n_1 > n_2$ and $x_1 - x_2 > 0$. The closer K to unity, the less significantly the maximum deviates from the middle of the isomorphous series.

Eqns (12) and (13) are valid only for ideal solid solutions, *i.e.*, provided that $K = \text{const}$. For non-ideal solid solutions, the distribution coefficient depends on the solution composition, which gives rise to a small shift in the maximum of the $x_1 - x_2$ difference.

The dependence of optical indicatrix characteristics on the composition of the crystal is a useful criterion of the ordering degree. The experimental determination of this dependence does not require complicated X-ray diffraction studies. It is reasonable to assume that the birefringence (or another appropriate characteristics of the optical indicatrix distortion) is directly proportional to the deviation of the structure from the disordered one, *i.e.*, to a first approximation,

$$\Delta n \sim x_1 - x_2.$$

In such a case, the functional correlation between the anomalous birefringence and the crystal composition is given by expres-

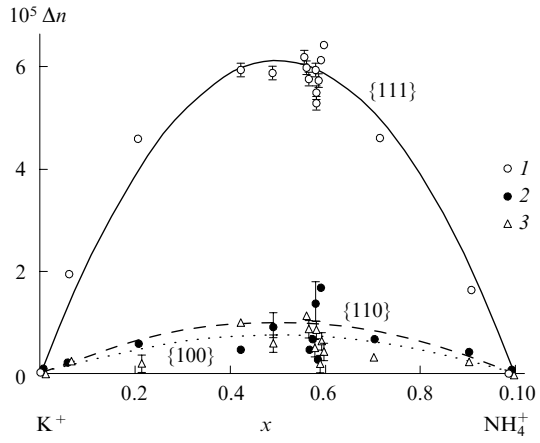


Figure 19. Anomalous birefringence as a function of stoichiometry for alum $[K_{1-x}(NH_4)_x]Al(SO_4)_2 \cdot 12\,H_2O$ crystals in the octahedral {111} (*1*), rhombododecahedral {110} (*2*) and cubic {100} (*3*) growth sectors.[32]

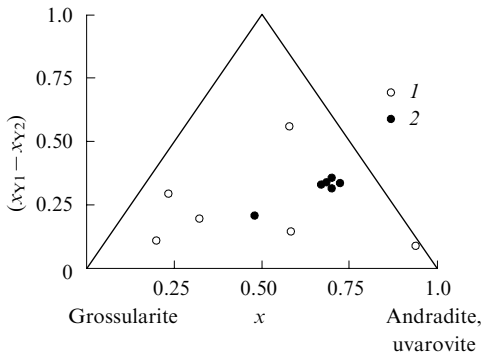


Figure 21. Difference in occupancy between two octahedral cationic sites as a function of the mean content of iron or chromium (x) for garnets of the grossularite–andradite (*1*) and grossularite–uvarovite (*2*) isomorphous series (assuming the orthorhombic space group *Fddd*).
The lines limit the region of possible crystal structures (corresponding to the maximum ordering degree); (*1*) from Refs 6, 9, 14–16, (*2*) from Ref. 17.

sions (12) and (13). When the ordering occurs over several sites, there will be no such a simple correlation, although a general trend of an increase in the ordering degree towards the middle of the isomorphous series will still be valid.

We surveyed the correlation between the anomalous birefringence and ordering degree from the one side and the crystal composition from the other side based on our own and literature data on three isomorphous alum series, *viz*., $(NH_4,K)Al(SO_4)_2 \cdot 12\,H_2O$, $K(Al,Cr)(SO_4)_2 \cdot 12\,H_2O$ and $NH_4(Al,Fe)(SO_4)_2 \cdot 12\,H_2O$,[29,32] sodium chlorate bromate crystals[27,28] and garnets of the grossularite–andradite isomorphous series.[13,15] A quasiparabolic function similar to that predicted theoretically is observed in all cases. As an example, the function anomalous birefringence *vs*. crystal composition for an alum isomorphous series with a common stoichiometry $(NH_4,K)Al(SO_4)_2 \cdot H_2O$ is plotted in Fig. 19. Additionally, it was demonstrated for a $[(NH_4)_{0.47}K_{0.53}](Al_{0.885}Cr_{0.115}) \cdot (SO_4)_2 \cdot 12\,H_2O$ crystal that the value of birefringence changes additively upon isomorphous substitutions in different sites.[156]

The naturally occurring garnets $Ca_3(Al,Fe,Cr)_2(SiO_4)_3$ represent a most striking example of the dissymmetrisation in crystals. However, a correlation between the birefringence and the aluminium to iron ratio for a series of crystals (according to data from several independent sources) looks like an array of data points limited from bottom with a straight line of zero birefringence and from top with a parabola-like curve with a maximum in the middle of the isomorphous series (Fig. 20) rather than a mere parabola. The ordering degrees of Al/Fe and Al/Cr cations in two octahedral sites of birefringent garnets reveal the same trend, according to all available (although rather scarce) crystal structure refinements (Fig. 21). Such a complex pattern is explained by the presence of crystals grown under very different conditions (primarily, at different temperatures) among the samples studied, which strongly affects the extent of optical anomalies (see Section VIII.5). If the correlation between the birefringence and the crystal composition is plotted for one crystal with compositional zoning, the theoretical parabola-like function is reproduced much better.

The ordering in the growth sectors of the tetrahedral faces in sodium chlorate bromate solid solutions occurs in two groups of sites containing one and three sites, respectively.[27] In such a case, the dependence of the ordering degree on the crystal composition should be asymmetric, according to expression (12). The experimental data nicely confirm the expected behaviour pattern (Fig. 22).

For the case of microisomorphism (*e.g*., minor admixtures of Al^{3+} and Fe^{3+} in quartz or of Cu^{2+} in $ZnSeO_4 \cdot 6\,H_2O$), Eqn (12) is substantially simplified. The degree of kinetic ordering becomes

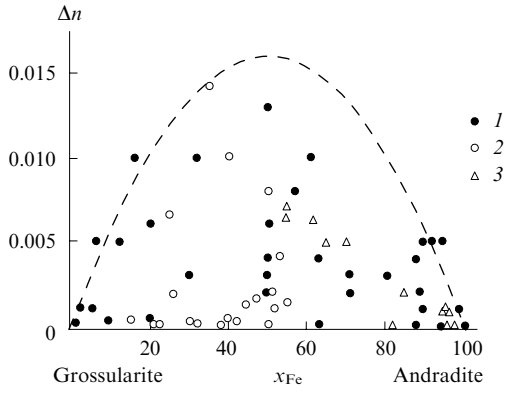


Figure 20. Birefringence as a function of the mean fraction of iron in the octahedral sites x_{Fe} for garnets of the grossularite–andradite isomorphous series.[32]
(*1*) Literature data by various authors, (*2*) our data, (*3*) data on a one-zoned crystal. For a better comparison with the theoretical prediction, a parabola is drawn with the dashed line.

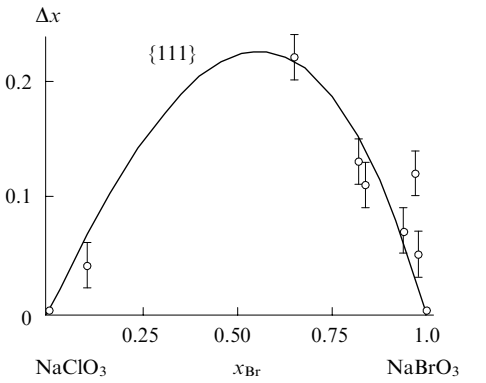


Figure 22. Difference in site occupancies as a function of the mean bromine content for the tetrahedral growth sectors of sodium chlorate bromate crystals (adapted from Ref. 27).
The line represents the result of calculations according to the formula (12) for $K = 0.4$.

Table 11. A comparison of parameters of different alum isomorphous series and the anomalous birefringence values for the octahedral growth sectors of the respective crystals.

Isomorphous series	Substitution site	Sign of Δn	$10^7 \lvert\Delta n_{max}\rvert$	δa /Å	δr /Å	δn
$(NH_4,K)Al(SO_4)_2 \cdot 12\,H_2O$	A^+	–	600 ± 30	0.082	0.10	0.0029
$(Rb,K)Al(SO_4)_2 \cdot 12\,H_2O$	A^+	–	540	0.085	0.14	0.0001
$(Rb,NH_4)Al(SO_4)_2 \cdot 12\,H_2O$	A^+	?	~ 0	0.003	0.04	0.0028
$(NH_4,K)Cr(SO_4)_2 \cdot 12\,H_2O$	A^+	–	> 70	0.078	0.10	0.0028
$(K,Rb)Cr(SO_4)_2 \cdot 12\,H_2O$	A^+	?	~ 0	0.083	0.14	0.0001
$K(Al,Cr)(SO_4)_2 \cdot 12\,H_2O$	M^{3+}	+	820 ± 30	0.038	0.09	0.0249
$NH_4(Al,Fe)(SO_4)_2 \cdot 12\,H_2O$	M^{3+}	+	550 ± 70	0.078	0.02	0.0254
$NH_4(Al,Cr)(SO_4)_2 \cdot 12\,H_2O$	M^{3+}	+	> 430	0.034	0.09	0.0248
$NH_4(Fe,Cr)(SO_4)_2 \cdot 12\,H_2O$	M^{3+}	?	~ 0	0.044	0.07	0.0006
$NH_4(Al,Ga)(SO_4)_2 \cdot 12\,H_2O$	M^{3+}	+	> 130	0.027	0.09	0.0090

Notes. The following notations are adopted: δa is the difference in the unit cell parameters between the end members of the isomorphous series; δr is the difference in the ionic radii (after Shannon [171]) of the isomorphous ions substituting each other; δn is the difference in the refraction indices between the end members of the isomorphous series.

directly proportional to the impurity concentration. Unfortunately, we are unaware of any experimental results supporting or disproving this conclusion.

According to a comparative analysis of characteristics of optical anomalies for ten isomorphous series of the same structural type (*viz*., alum, Table 11), the optical sign is unambiguously defined by the site subject to substitution.[32] The maximum birefringence strongly varies between the series showing no apparent correlation with the difference in substituting cation radii, unit cell parameters or refraction indices of the end members of the series.

The degree of ordering of atoms or vacancies in a specific crystallographic site can also be affected by admixtures occupying other sites in the crystal. Experimental data on this phenomenon are rather scarce and its origin is unclear. This can be illustrated with the experimentally observed influence exerted by some impurities on the ordering of Si and Al in synthetic cordierites. Various admixtures occupying different structural sites were tested, such as Be, Cs, Ca, Mn, Ti, Li, Cu, B, Sc, V, Cr and Fe.[45,46] Cordierites $Mg_2Al_2Si(Al_2Si_4O_{18})$ can undergo a phase transition from the hexagonal (space group *P*6/*mcc*) into the orthorhombic (space group *Cccm*) modifications. This transformation can occur both as a usual thermodynamic phase transition under specific $P-T$ conditions and as a kinetic phase transition under other conditions. The latter transition relates to the ordering of aluminium and silicon in three groups of the SiO_4 tetrahedra.[43] It turned out that the ordering degree is a function of the crystal composition. In particular, an increase in the concentration of such admixtures as Be, Al, Sc or B in the crystal gives rise to a decrease in the ordering degree and to the formation of hexagonal crystals. Indeed, no dissymmetrisation occurs or it is manifested to an insignificant extent in beryllium indialite $Mg_2(Al,Be)_3Si_6O_{18}$, indialite $Mg_2Al_4Si_5O_{18}$ and beryl $Al_2Be_3.(Si_6O_{18})$ crystals, which are isostructured to cordierite.[48,50–52] To the contrary, the introduction of Cs, Rb, Li and Cr admixtures enhances the ordering degree. However, it has to be noted that the exact composition of admixtures affects not only the kinetic Al/Si ordering, but the thermodynamic parameters of the equilibrium phase transition as well, which complicates the interpretation of the above data.

The heavy water substitution for a substantial fraction ($\sim 70\%$) of normal water in alum $K(Al,Cr)(SO_4)_2 \cdot 12\,H_2O$ crystals results in a substantial (severalfold) attenuation of the anomalous birefringence. The mechanism of this process remains unexplored.

2. Crystallisation medium composition

Atoms and admixtures present in the crystallisation medium but not incorporated in the crystal also affect the kinetic ordering. This influence can be illustrated with garnets of the grossularite–andradite isomorphous series as an example. As has been established in experiments devoted to the hydrothermal synthesis of garnets,[172] the birefringence shows an evident correlation with the crystallisation medium composition. In particular, the use of CaO or $Ca(OH)_2$ instead of $CaCO_3$ as a calcium source attenuates the birefringence. Furthermore, Na_2CO_3 aqueous solution as a solvent provides a higher birefringence than Na_2SiO_3 or $Na_2B_4O_7$ solutions. The amount of CO_2 and H_2O in the load for the hydrothermal synthesis of garnets also affects the emergence of optical anomalies.[155] For instance, if the synthesis is accomplished at a temperature of 650 °C and a pressure of 800 bar, the presence of 10% of water in the load gives rise to optical anomalies, whereas no anomalies were observed for the water content at a 5% level. Crystals with optical anomalies can also be grown from CO_2- and H_2O-free media. The mechanism of this correlation between the anomalous birefringence and medium composition has not been elucidated in sufficient detail so far.

3. Temperature and pressure

The dependence of the difference of site occupancies $(x_1 - x_2)$ and, consequently, of the degree of distortion of the optical indicatrix on the crystal growth temperature can be deduced theoretically. The distribution coefficient is characterised by the Arrhenius-type exponential temperature dependence [122]

$$K_i = K_i^{\#} \exp\left(-\frac{U_i}{RT}\right), \tag{14}$$

where $K_i^{\#}$ is the preexponential factor, U_i includes the energy of elastic deformations and the mixing energy due to the substitution in the crystal, $i = 1, 2$. After substitution of (14) into Eqn (12), one gets a rather complicated expression, which is not given here. However, it can be demonstrated that the difference in site occupancies decreases with an increase in temperature. A more prominent asymptotic dependence comes into effect when the distribution coefficient approaches unity, *i.e*., the difference of site occupancies becomes small. In such a case, an inversed correlation of the difference of site occupancies on temperature is afforded [32]

$$x_1 - x_2 \approx x(1-x)\left(\frac{U_1 - U_2}{RT}\right). \tag{15}$$

Thus according to theoretical predictions, the ordering degree should decrease with an increase in the crystal growth temperature. Physically, this correlation means that the energy of atomic vibrations becomes comparable with the energy difference between non-equivalent sites at elevated temperatures. Respectively, the selectivity of the incorporation of isomorphous atoms is

weakened, which gives rise to a lower degree of the ordering. In addition to this effect, the diffusion relaxation processes and the annealing of the ordered distribution of atoms directly in the course of the growth and in the post-growth period are accelerated at elevated temperatures (see Sections V and VII).

The attenuation of the kinetic ordering and optical anomalies with an increase in the growth temperature were observed and elucidated experimentally for alum [32, 156] (Fig. 23) and quartz crystals.[77, 79] Furthermore, the absence of optical anomalies for crystals grown at a sufficiently high temperature was registered for garnets of the grossularite–andradite isomorphous series [155, 173] (Fig. 24) and cordierites.[43]

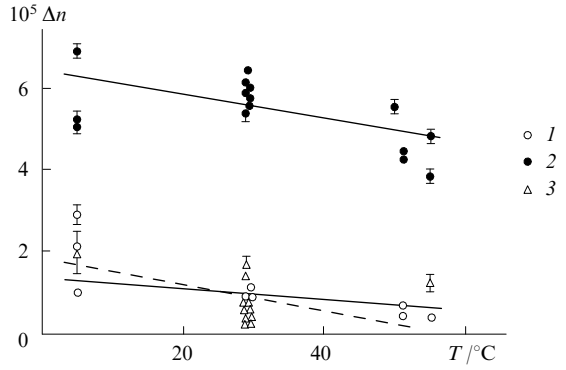


Figure 23. Anomalous birefringence as a function of the growth temperature for three growth sectors of alum $[K_{0.51-0.40}(NH_4)_{0.49-0.60}]Al.(SO_4)_2\cdot 12\,H_2O$ crystals.[155]
The measurements were accomplished for cuts along the (110) plane.
The growth sectors: (*1*) {100}, (*2*) {111}, (*3*) {110}.

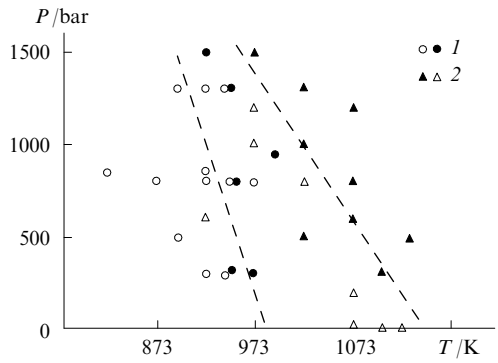


Figure 24. The regions of formation of isotropic (shaded symbols) and anisotropic (plain symbols) crystals of garnets of the grossularite–andradite isomorphous series in the P, T coordinates (tentatively divided by dashed lines).[156]
(*1*) Artificial crystals, (*2*) naturally occurring crystals.

Experimental data on the influence of pressure on optical anomalies are very scarce. We are aware of only one such example concerning garnets of the grossularite–andradite series (see Fig. 24). In that study, a trend to an increase in the optical anomalies with an increase in pressure was revealed.[155]

Apparently, it is variations in the $P-T$ conditions of the crystal growth that are responsible for the lack of a strict correlation between the anomalous birefringence of grandite crystals and their composition as regards the Al/Fe ratio (see Section VIII.1 and Fig. 20), which explains the fact that all experimental points fall into the area limited from the top by the theoretical parabola.

4. Growth rate

The kinetic ordering of atoms and resultant optical anomalies should attenuate with an increase in the crystal growth rate. This reflects the fact that the conditions for the statistical selection of atoms on the surface of a growing face get worse at higher crystallisation rates. Since the incorporation of atoms into the crystal obeys to a large extent the trial-and-error statistics,[122] the components do not have enough time to settle in ordered positions before the surface layer gets buried in the bulk of the crystal. This means that a state that is not equilibrium with respect to the growing crystal surface gets buried (however, this state can appear much closer to the equilibrium state with respect to the bulk). This effect was observed experimentally for a number of natural minerals [47] prone to ordinary thermodynamic order–disorder phase transitions [feldspars $KAlSi_3O_8$, omphacite $(Ca,Na)(Mg,Fe,Al)Si_2O_6$, dolomite $CaMg(CO_3)_2$].

The attenuation of dissymmetrisation-induced optical anomalies with an increase in the crystal growth rate was also reported for analcime $NaAlSi_2O_6\cdot 2H_2O$.[23] A detailed analysis devoted to the dependence of the birefringence on the growth rate in alum $(K,NH_4)Al(SO_4)_2\cdot 12H_2O$ crystals [32] revealed no correlation (Fig. 25*a*) over a wide range of growth rates. On the other hand, an evident trend towards a decrease in the birefringence with an increase in the growth rate was confirmed for crystals of another isomorphous alum series, *viz*., $K(Al,Cr)(SO_4)_2\cdot 12H_2O$ (Fig. 25*b*). Therefore, the effect of the growth rate on optical anomalies can indeed be detected but it is insignificant in some cases.

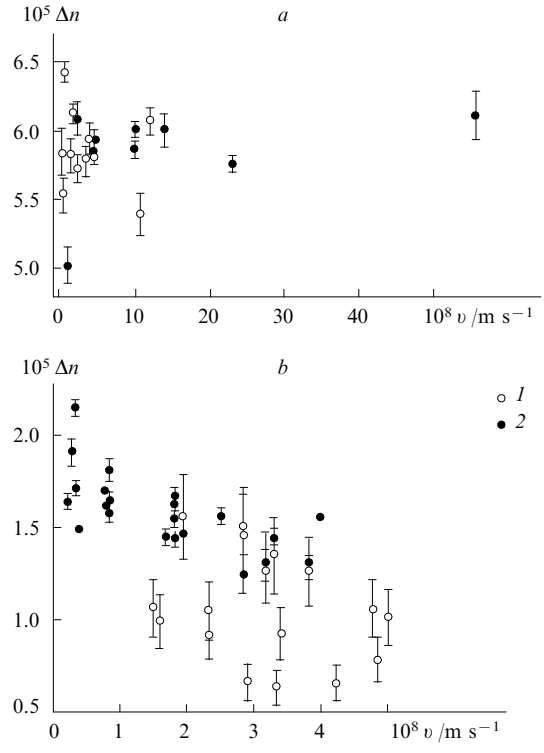


Figure 25. Anomalous birefringence as a function of the growth rate for alum crystals.[32]
(*a*) The isomorphous series of solid solutions $[K_{1-x}(NH_4)_x]Al.(SO_4)_2\cdot 12\,H_2O$: (*1*) $x = 0.55-0.60$ ($T = 28-30$ °C); (*2*) $x = 0.36-0.42$ ($T = 29.5-32$ °C); (*b*) $K(Al_{1-x}Cr_x)(SO_4)_2\cdot 12\,H_2O$: (*1*) $x = 0.03-0.05$ ($T = 24-37$ °C); (*2*) $x = 0.04-0.05$ ($T = 34-36$ °C). The crystals were grown under conditions of free convection (plain symbols) or stirring (shaded symbols) at a Reynolds number of 1400–3200.[29]

The kinetic disordering (which is the inverse process with respect to the growth dissymmetrisation) occurring within the stability range of ordered solid solutions, was treated theoretically for the cases of crystallisation from both vapour [1, 2, 174] and melt.[175] In these studies, the growth of a binary Kossel crystal composed of equal proportions of particles A and B was simulated for the case of the following pairwise interaction energies: $\varepsilon_{AA} = \varepsilon_{BB}$ and $\varepsilon_{AB} = \varepsilon_{BA} = \psi\varepsilon_{AA}$. This effect should attenuate the growth ordering with an increase in the crystal growth rate. According to our calculations [32] performed within the model proposed by Chernov,[1] the deviation of the ordering degree from the equilibrium value becomes negligibly small when a crystal grows in a nearly equilibrium mode (although the solution supersaturation can be as high as 0.3) and $\psi = 2$. It has to be noted that this model is rather rough, since it assumes strong collective interactions between neighbouring atoms together with a significant positive non-ideality of the solid solution. Although in the majority of real cases, crystals prone to the growth dissymmetrisation are nearly ideal solid solutions, for which $\psi \to 1$ and the Chernov's equations do not hold. As an alternative to this approach, the problem can be treated within the theory of absolute reaction rates. This approach is based on the dependence of the distribution coefficient on the crystal growth rate (*i.e.*, the solution supersaturation).[1, 122, 176] According to the theoretical analysis, the dissymmetrisation-induced ordering degree should be inversely proportional to the solution supersaturation; however, no experimental result on this subject is available.

5. Hydrodynamics and mass transfer in the solution

Experimental data on the influence of hydrodynamics and mass transfer in the mother liquor on the dissymmetrisation-induced optical anomalies are available only for alum crystals.[32] No correlation between the value of anomalous birefringence and mass transfer coefficient against the background of a large scatter among the experimental points was revealed for an extended set of crystals from two isomorphous series, $(K,NH_4)Al(SO_4)_2 \cdot 12H_2O$ and $K(Al,Cr)(SO_4)_2 \cdot 12H_2O$, grown under different hydrodynamic conditions. A dramatic change in the mixing regime of the mother liquor (from the natural convection to an intense stirring) produced no effect on the anomalous birefringence in one crystal grown from the solution. This lack of significant influence indicates that it is the processes on the surface of the crystal that play the key role in the emergence of optical anomalies in alum crystals, which is in accord with the hypothesis of the kinetic ordering of atoms.

Meanwhile, the mass transfer conditions can strongly affect the inhomogeneity of the distribution of optical anomalies over the crystal. This influence is manifested in the formation of a more complex vicinal topology upon specific hydrodynamic conditions of the mother liquor (which results in a complicated pattern of the subsectorial structure of the crystal). Additionally, the mixing conditions affect the character of the birefringence trend.[33, 149]

IX. Conclusion

The comprehensive analysis of kinetic ordering phase transitions that give rise to the dissymmetrisation of crystalline solid solutions demonstrates their obvious difference from the classical polymorphous transformations. The symmetry and the structure of a growing crystal face are clearly distinguished from those of the bulk crystal, which enables the emergence of ordering of structural units on the growing surface, which can be transferred to the bulk under certain conditions. Therefore, it is the selective adsorption of solid solution components by a growing crystal that acts as the control parameter of this phase transition. This fact determines major specific features of the kinetic ordering phase transitions.

The state of the surface and the kinetics of adsorption of components in the course of the crystal growth cannot be characterised by a single parameter, since they are affected by both usual thermodynamic parameters (temperature, pressure, chemical potentials of the components) and specific kinetic parameters (growth rate, peculiarities of the surface microtopography). As a result, one compound under similar crystallisation conditions can yield a variety of structures characterised by different symmetries and ordering degrees. Therefore, the classical question concerning the symmetry and structure of analcime crystals: 'Is each analcime different?' ‡ can be answered positively. And this is valid not only for analcime but for the majority of inorganic crystalline solid solutions.

In addition to the aspects mentioned above, it has to be noted that the kinetic ordering of atoms is always metastable and can be converted into the equilibrium disordered state by means of high-temperature annealing. Furthermore, the annealing can be actuated directly during the growth process or just after it, which additionally increases the complexity of possible transient crystal structures.

Since the mechanism of the kinetic ordering differs strongly from that of the ordinary equilibrium ordering, both these phenomena can be manifested in a crystal simultaneously. Thus the kinetic ordering can occur in crystals with negative (the components tend to order), zero or even positive (the components tend to segregate up to the emergence of a miscibility gap) energies of mixing of components constituting a solid solution. As an example of this apparent contradiction, sodium chlorate bromate crystals can be mentioned, which are characterised by a significant positive energy of mixing of components (with a possible emergence of a miscibility gap [177]) but simultaneously manifest distinct kinetic ordering of the $HalO_3^-$ anions.[28]

Kinetic phase transitions are very common, they are typical of virtually any crystalline solid solutions. However, this phenomenon remains largely unexplored, despite the long history of its studies. Over the last decade, the structural origins of the dissymmetrisation have been elucidated and methods for the analysis of symmetry in crystals with anomalous optical properties based on X-ray diffraction data have been developed, with the active involvement of the authors of the present review. A large body of information on the actually occurring ordering patterns, effects of the crystal composition, the role of high-temperature annealing, reasons for the inhomogeneity of the spatial distribution of regions with different degrees of ordering over a crystal have been analysed quite thoroughly (although not comprehensively). Still, the issues related to the influence exerted by the chemical composition of dopant structural units and the growth conditions, primarily, temperature and the growth rate, on the growth ordering have not been addressed adequately. Furthermore, the validity of the suggested mechanism of the growth dissymmetrisation has been supported only by indirect data, whereas no direct confirmations have been obtained so far. This is mainly due to the insufficient power of presently available experimental techniques for the real-time structural monitoring of surface layers of growing crystals. Therefore, the story concerning the growth dissymmetrisation mechanism should be continued.

This work was performed with a partial financial support from the Russian Foundation for Basic Research (Project No. 05-05-64 289) and INTAS YS Fellowship Program (Grant 2004-83-2826).

References

1. A A Chernov *Usp. Fiz. Nauk* **100** 277 (1970) [a]
2. A A Chernov *Zh. Eksp. Teor. Fiz.* **53** 2090 (1967) [b]
3. A Putnis, J D C McConnell *Principles of Mineral Behaviour* (Oxford, London: Blackwell, 1980)
4. R W Bené *J. Appl. Phys.* **61** 1826 (1987)
5. K N Tu, S R Herd, U Gösele *Phys. Rev. B* **43** 1198 (1991)

‡ The title of the paper by Mazzi and Galli.[22]

6. Y Takéuchi, N Haga, S Umizu, G Sato *Z. Kristallogr.* **158** 53 (1982)
7. M Akizuki *Am. Mineral.* **69** 328 (1984)
8. F M Allen, P R Buseck *Am. Mineral.* **73** 568 (1988)
9. K J Kingma, J W Downs *Am. Mineral.* **74** 1307 (1989)
10. D T Griffen, D M Hatch, W R Phillips, S Kulaksiz *Am. Mineral.* **77** 399 (1992)
11. B P McAloon, A M Hofmeister *Am. Mineral.* **78** 957 (1993)
12. B P McAloon, A M Hofmeister *Am. Mineral.* **80** 1145 (1995)
13. A G Shtukenberg, Yu O Punin, O V Frank-Kamenetskaya, O G Kovalev, P B Sokolov *Mineral. Mag.* **65** 445 (2001)
14. A G Shtukenberg, D Yu Popov, Yu O Punin *Mineral. Mag.* **66** 275 (2002)
15. A G Shtukenberg, Yu O Punin *Opticheskie Anomalii v Kristallakh* (Optical Anomalies in Crystals) (St Petersburg: Nauka, 2004)
16. A G Shtukenberg, D Yu Popov, Yu O Punin *Mineral. Mag.* **69** 539 (2005)
17. M Wildner, M Andrut *Am. Mineral.* **86** 1231 (2001)
18. M Andrut, M Wildner *Am. Mineral.* **86** 1219 (2001)
19. G Balestrino, P Paroli, S Geller *Phys. Rev. B* **34** 8104 (1986)
20. K Kitamura, N Iyi, S Kimura, F Cherrier, J M Davignes, H Le Gall *J. Appl. Phys.* **60** 1486 (1986)
21. K Kitamura, S Kimura, J M Davignes, H Le Gall *J. Cryst. Growth* **74** 453 (1986)
22. F Mazzi, E Galli *Am. Mineral.* **63** 448 (1978)
23. M Akizuki *Am. Mineral.* **66** 403 (1981)
24. O V Frank-Kamenetskaya, I V Rozhdestvenskaya, I I Bannova, A V Kostitsyna, T N Kaminskaya, V V Gordienko *Kristallografiya* **40** 698 (1995) [c]
25. O V Frank-Kamenetskaya, I V Rozhdestvenskaya *Atomarnye Defekty i Kristallicheskaya Struktura Mineralov. Kristallokhimiya (Itogi Nauki i Tekhniki)* [Atomic Defects and Crystal Structure of Minerals. Crystal Chemistry (Advanced in Science and Engineering Series)] (Moscow: Kosmosinform, 2001)] Vol. 33
26. P S H Gopalan, M L Peterson, G Crundwell, B Kahr *J. Am. Chem. Soc.* **115** 3366 (1993)
27. G Crundwell, P Gopalan, A Bakulin, M L Peterson, B Kahr *Acta Crystallogr., Sect. B* **53** 189 (1997)
28. A G Shtukenberg, I V Rozhdestvenskaya, D Yu Popov, Yu O Punin *J. Solid State Chem.* **177** 4732 (2004)
29. A G Shtukenberg, Yu O Punin, E N Kotel'nikova, S M Sukharzhevskii *Zh. Strukt. Khim.* **35** (5) 60 (1994) [d]
30. A G Shtukenberg, O V Frank-Kamenetskaya, I I Bannova, I V Rozhdestvenskaya, S V Kulakova, T I Ivanova, Yu O Punin *Kristallografiya* **45** 999 (2000) [c]
31. H Euler, A Kirfel, H Klapper, A Stukenberg *Z. Kristallogr.* (Suppl. Issue 16) 30 (1999)
32. A G Shtukenberg, Yu O Punin, V N Soloviev *Mineral. Mag.* **64** 837 (2000)
33. A G Shtukenberg, Yu O Punin, E Haegele, H Klapper *Phys. Chem. Miner.* **28** 665 (2001)
34. I V Rozhdestvenskaya, O V Frank-Kamenetskaya, A G Shtukenberg, I I Bannova *Zh. Strukt. Khim.* **42** 753 (2001) [d]
35. P S H Gopalan, B Kahr *J. Solid State Chem.* **107** 563 (1993)
36. A G Shtukenberg *J. Solid State Chem.* **178** 2608 (2005)
37. M Akizuki, H Konno *Neues Jahrb. Mineral., Abh.* **151** 99 (1985)
38. M Akizuki, T Terada *Neues Jahrb. Mineral., Mh.* (5) 234 (1998)
39. B Kahr, J M McBride *Angew. Chem. Int. Ed. Engl.* **31** 1 (1992)
40. F M Allen, C Burnham *Can. Mineral.* **30** 1 (1992)
41. M Ohkawa, A Yoshiase, S Takeno *Mineral J.* **17** 1 (1994)
42. T Tanaka, M Akizuki, Y Kudoh *Mineral. Mag.* **66** 261 (2002)
43. L I Tsinober, M I Samoilovich, T V Demina, A A Bobr-Sergeev *Kristallografiya* **22** 354 (1977) [d]
44. L I Tsinober, M I Samoilovich *Dokl. Akad. Nauk SSSR* **242** 1337 (1978) [e]
45. T V Demina *Zap. Vsesoyuzn. Mineralog. O-va* **109** (1) 37 (1980)
46. T V Demina, Candidate Thesis in Geological-mineralogical Sciences, Institute of Geology, Novosibirsk, 1980
47. M A Carpenter, A Putnis, in *Metamorphic Reactions. Kinetics, Textures, and Deformation* (Eds A B Thompson, D C Rubie) (Berlin: Springer, 1985) p. 1
48. T V Demina *Zap. Vsesoyuzn. Mineralog. O-va* **119** (4) 74 (1990)
49. T V Demina, G G Afonina *Zap. Vsesoyuzn. Mineralog. O-va* **123** (6) 59 (1994)
50. T V Demina, M A Mikhailov *Zap. Vsesoyuzn. Mineralog. O-va* **129** (5) 81 (2000)
51. T V Demina, M A Mikhailov *Zap. Vsesoyuzn. Mineralog. O-va* **130** (2) 114 (2001)
52. S G Pecherskaya, M A Mikhailov, T V Demina, L A Bogdanova, O Yu Belozerova *Kristallografiya* **48** 407 (2003) [c]
53. T V Demina, M A Mikhailov, O Yu Belozerova *Zap. Vsesoyuzn. Mineralog. O-va* **132** (5) 1 (2003)
54. T V Demina *Izv. Akad. Nauk, Ser. Fiz.* **68** 621 (2004) [f]
55. M Akizuki, T Kuribayashi, T Nagase, A Kitakaze *Am. Mineral.* **86** 364 (2001)
56. A G Shtukenberg, I V Rozhdestvenskaya, Yu M Bronzova, O V Frank-Kamenetskaya, A A Zolotarev, I I Bannova, in *Mineralogicheskie Muzei (Tezisy Dokladov Konferentsii), Sankt-Peterburg, 2005* [Mineralogical Museums (Abstracts of Reports of the Conference), St Petersburg, 2005] p. 265
57. M Akizuki *Am. Mineral.* **71** 1510 (1986)
58. T Tanaka, R Kimura, M Akizuki, Y Kudoh *Mineral. Mag.* **66** 409 (2002)
59. J M McBride, S B Bertman *Angew. Chem., Int. Ed. Engl.* **28** 330 (1989)
60. I Weissbuch, L Addadi, M Lahav, L Leiserowitz *Science* **253** 593 (1991)
61. I Weissbuch, R Popovitz-Biro, M Lahav, L Leiserowitz *Acta Crystallogr., Sect. B* **51** 115 (1995)
62. U Cheison, in *Polevye Shpaty* (Feldspars) (Translated into Russian; Moscow: Izd. Inostr. Lit., 1952) p. 295
63. M Akizuki, I Sunagawa *Mineral. Mag.* **42** 453 (1978)
64. M Akizuki *Neues Jahrb. Mineral., Mh.* 181 (1981)
65. M Vaida, L J W Shimon, Y Weisinger-Lewin, F Frolow, M Lahav, L Leiserowitz, R K McMullan *Science* **241** 1475 (1988)
66. J M McBride *Angew. Chem., Int. Ed. Engl.* **28** 377 (1989)
67. M Akizuki *Am. Mineral.* **72** 645 (1987)
68. M Akizuki, Ya Kudoh, T Kuribayashi *Am. Mineral.* **81** 1507 (1996)
69. M Akizuki, M C Hampar, J Zussman *Mineral. Mag.* **43** 237 (1979)
70. J B Parise, C Cuff, F H Moore *Mineral. Mag.* **43** 943 (1980)
71. K Shinoda, N Aikawa *Phys. Chem. Miner.* **21** 21 (1994)
72. K Shinoda, N Aikawa, in *Abstracts of the 16th General Meeting of International Mineralogical Association, Pisa, 1994* p. 373
73. M Akizuki *Mineral. Mag.* **51** 615 (1987)
74. T I Barry, W J Moore *Science* **144** 289 (1964)
75. T M Barry, P McNamara, W J Moore *J. Chem. Phys.* **42** 2599 (1965)
76. L I Tsinober, M I Samoilovich, L A Gordienko, L G Chentsova *Kristallografiya* **12** 65 (1967) [c]
77. L I Tsinober, M I Samoilovich, V E Khadzhi, M V Lelekova *Dokl. Akad. Nauk SSSR* **176** 676 (1967) [e]
78. M I Samoilovich, L I Tsinober, V E Khadzhi, M V Lelekova *Kristallografiya* **13** 850 (1968) [c]
79. L I Tsinober, M I Samoilovich, in *Problemy Sovremennoi Kristallografii* (The Problems of Modern Crystallography) (Ed. A A Chernov) (Moscow: Nauka, 1975) p. 207
80. V M Vinokurov, G R Bulka, N M Nizamutdinov, N M Khasanova *Dokl. Akad. Nauk SSSR* **237** 1388 (1977) [e]
81. N M Nizamutdinov, G R Bulka, N M Khasanova, V D Shchepkin, V M Vinokurov *Kristallografiya* **22** 775 (1977) [c]
82. A M Anufriev, G R Bulka, V M Vinokurov, G A Krinari, N M Nizamutdinov, M A Urasin, N M Khasanova, in *Neodnorodnost' Mineralov i Rost Kristallov (Materialy 11 S'ezda MMA)* [Heterogeneity of Minerals and Growth of Crystals (Proceedings of the 11th Congress of MMA)] (Moscow: Nauka, 1980) p. 10
83. G R Bulka, V M Vinokurov, N M Nizamutdinov, N M Hasanova *Phys. Chem. Miner.* **6** 283 (1980)
84. S Geschwind, J P Remeika *Phys. Rev.* **122** 757 (1961)
85. S A Marshall, A R Reinberg *Phys. Rev.* **132** 134 (1963)
86. N M Nizamutdinov, G R Bulka, N M Gainullina, V M Vinokurov, in *Fizicheskie Svoistva Mineralov i Gornykh Porod* (Physical Properties of Minerals and Rocks) (Ed. V M Vinokurov) (Kazan: Kazan State University, 1976) p. 3

87. M Akizuki *Am. Mineral.* **74** 859 (1989)
88. V I Stepanov, V A Moleva *Zap. Vsesoyuzn. Mineralog. O-va* **2** 556 (1962)
89. A F Konstantinova, A N Stepanov, L A Korostel', A V Kornilov, N A Kulagin, G R Otobaev *Kristallografiya* **38** 194 (1993) [c]
90. R Brauns *Die Optischen Anomalien der Kristalle* (Leipzig: Preisschr. Jablonowski-Ges., 1891)
91. L A Vardanyants *Zap. Vseros. Mineralog. O-va* **1** 16 (1941)
92. J Takano, K Takano *J. Geol. Soc. Jpn.* **65** 236 (1959)
93. S E Frood, B A Mills *Am. Mineral.* **63** 316 (1978)
94. J M Hughes, M Cameron, A N Mariano *Am. Mineral.* **76** 1165 (1991)
95. J M Hughes, M Cameron, K D Crowley *Am. Mineral.* **76** 1857 (1991)
96. J Rakovan, R J Reeder *Am. Mineral.* **79** 892 (1994)
97. M Akizuki, H Nisidon, Y Kudon, T Watanabe, K Kurata *Mineral. Mag.* **58** 307 (1994)
98. J Rakovan, in *Reviews in Mineralogy and Geochemistry. Phosphates: Geochemical, Geobiological and Materials Importance* Vol. 48 (Eds M J Kohn, J Rakovan, J M Hughes) (Washington, DC: MSA, 2002) p. 51
99. I I Shafranovskii, V I Mikheev, V A Mokievskii *Zap. Vsesoyuzn. Mineralog. O-va* **1** 28 (1952)
100. H Strunz, H Wilk *Z. Dtsch. Gemmol. Ges.* **23** 2 142 (1974)
101. S A Anan'ev, S I Konovalenko *Geol. Geofiz.* **9** 97 (1984)
102. A A Zolotarev, Z T Dzhuraev, I V Pekov, K V Mikhailova *Zap. Vseros. Mineralog. O-va* **129** (2) 64 (2000)
103. R J Reeder, in *Reviews in Mineralogy* Vol. 27 (Ed. R J Reeder) (Washington, DC: MSA, 1992) p. 381
104. M B Chistyakova, G A Osolodkina, Z P Razmanova *Dokl. Akad. Nauk SSSR* **159** 1305 (1964) [e]
105. D S Goldman, G R Rossman *Am. Mineral.* **63** 490 (1978)
106. T Armbruster, R Oberhansli *Am. Mineral.* **73** 585 (1988)
107. A N Karnozhitskii *Zap. Imper. S-Pb. Mineralog. O-va* **27** 209 (1891)
108. M Akizuki *Lithos* **14** 17 (1981)
109. M Akizuki, H Konno *Mineral. Mag.* **51** 427 (1987)
110. M Akizuki, H Nishido, M Fujimoto *Am. Mineral.* **74** 1337 (1989)
111. N Yu Ikornikova-Lemmlein *Dokl. Akad. Nauk SSSR* **53** 255 (1946) [e]
112. M Akizuki *Am. Mineral.* **70** 822 (1985)
113. M Akizuki, K Harada *Am. Mineral.* **73** 613 (1988)
114. M Akizuki *Can. Mineral.* **25** 707 (1987)
115. P H Ribbe, in *Reviews in Mineralogy* Vol. 5 (Washington, DC: MSA, 1980) p. 171
116. M Akizuki, H Konno *Am. Mineral.* **70** 814 (1985)
117. M Akizuki, Ya Kudoh, Y Satoh *Eur. J. Mineral.* **5** 839 (1993)
118. E Dowty *Am. Mineral.* **61** 460 (1976)
119. M Akizuki, H Nishido *Am. Mineral.* **73** 1434 (1988)
120. G R Rossman, R D Aines *Am. Mineral.* **71** 779 (1986)
121. A V Shubnikov *Kristallografiya* **6** 319 (1961) [c]
122. A A Chernov, E I Givargizov, Kh S Bagdasarov, V A Kuznetsov, L N Dem'yanets, A N Lobachev *Sovremennaya Kristallografiya* (Modern Crystallography) (Moscow: Nauka, 1980) Vol. 3
123. G Nikolis, I Prigogine *Self-organization in Nonequilibrium Systems* (New York: Wiley, 1977)
124. H Haken *Information and Self-organization* (Berlin: Springer, 1988)
125. P M Goryankov, G Yu Ivanyuk *Samoorganizatsiya Mineral'nykh Sistem* (Self-organisation of Mineral Systems) (Moscow: GEOS, 2001)
126. J F Nye *Physical Properties of Crystals. Their Representation by Tensors and Matrices* (Oxford: Oxford University Press, 1985)
127. T A Zakharchenko, in *Fizicheskie Svoistva Mineralov i Gornykh Porod* (Physical Properties of Minerals and Rocks) (Ed. V M Vinokurov) (Kazan: Kazan State University, 1976) p. 97
128. D Pohl *Acta Crystallogr., Sect. A* **34** 574 (1978)
129. R N Abbott Jr *Am. Mineral.* **78** 952 (1993)
130. R N Abbott Jr *Can. Mineral.* **32** 909 (1994)
131. R N Abbott Jr *Can. Mineral.* **34** 595 (1996)
132. G A Lager, T Armbruster, D Pohl *Phys. Chem. Miner.* **14** 177 (1987)
133. D Yu Popov *Kristallografiya* **47** 893 (2002) [c]
134. D Yu Popov, O A Popova *Kristallografiya* **49** 932 (2004) [c]
135. A Putnis, D L Bish *Am. Mineral.* **68** 60 (1983)
136. P Seiler *Accurate Molecular Structures. Their Determination and Importance* (Eds A Domenicano, I Hargittai) (Oxford: Oxford University Press, 1992)
137. H S Yoder Jr *J. Geol.* **58** 221 (1950)
138. Y Takéuchi, N Haga *Proc. Jpn. Acad.* **52** 228 (1976)
139. I V Rozhdestvenskaya, O V Frank-Kamenetskaya, O G Kovalev, I I Bannova, Yu O Punin, in *Rentgenografiya Mineral'nogo Syr'ya (Tezisy Dokladov 14 Mezhdunarodnoi Konferentsii), Sankt-Peterburg, 1999* [X-Ray diffractometry of Minerals (Abstracts of Reports of the 14th International Conference), St Petersburg, 1999] p. 112
140. E Rossmanith, Th Armbruster *Z. Kristallogr.* **210** 645 (1995)
141. H Kroll, T Lueder, H Schlenz, A Kirfel, T Vad *Eur. J. Mineral.* **9** 705 (1997)
142. R Heinemann, V Staack, A Fisher, H Kroll, T Vad, A Kirfel *Am. Mineral.* **84** 1400 (1999)
143. M Merli, L Ungaretti, R Oberti *Am. Mineral.* **85** 532 (2000)
144. A Kifrel *Phys. Chem. Miner.* **23** 503 (1996)
145. B K Vainshtein *Sovremennaya Kristallografiya* (Modern Crystallography) (Moscow: Nauka, 1979) Vol. 1
146. N M Nizamutdinov, G R Bulka, N M Gainullina, V M Vinokurov, in *Fizicheskie Svoistva Mineralov i Gornykh Porod* (Physical Properties of Minerals and Rocks) (Ed. V M Vinokurov) (Kazan: Kazan State University, 1976) p. 49
147. M Akizuki, Y Takéuchi, T Terada, Y Kudoh *Neues Jahrb. Mineral., Mh.* (12) 565 (1998)
148. S Gali *Z. Kristallogr.* **163** 43 (1983)
149. A G Shtukenberg, Yu O Punin *Neues Jahrb. Mineral., Mh.* (6) 241 (2003)
150. G A Novak, G V Gibbs *Am. Mineral.* **56** 791 (1971)
151. T Armbruster, C A Geiger, G A Lager *Am. Mineral.* **77** 512 (1992)
152. J R Smyth, R E Madel, T C McCormick, J L Munoz, G R Rossman *Am. Mineral.* **75** 314 (1990)
153. R Basso, F Cimmino, B Messiga *Neues Jahrb. Mineral., Abh.* **150** 247 (1984)
154. I Náray-Szabó *Z. Kristallogr. Kristallgeom. Kristallphys. Kristallchem.* **99** 291 (1938)
155. Y Hariya, M Kimura *J. Fac. Sci., Hokkaido Univ., Ser. IV* **18** 611 (1978)
156. A G Shtukenberg, Yu O Punin, O G Kovalev *Kristallografiya* **43** 505 (1998) [c]
157. A Lasaga, in *Kinetics of Geochemical Processes. Reviews in Mineralogy* Vol. 8 (Eds A C Lasaga, R J Kirkpatrick) (Washington, DC: MSA, 1981) p. 261
158. J P Poirier *Creep of Crystals: High Temperature Deformation Processes in Metals, Ceramics and Minerals* (Cambridge, New York: Cambridge University Press, 1985)
159. S Chakraborty, J Ganguly *Contrib. Mineral. Petrol.* **111** 74 (1992)
160. R Freer, A Edwards *Contrib. Mineral. Petrol.* **134** 370 (1999)
161. C S Schwandt, R T Cygan, H R Westrich *Am. Mineral.* **80** 438 (1995)
162. C S Schwandt, R T Cygan, H R Westrich *Am. Mineral.* **81** 448 (1996)
163. P Ya Azimov, Candidate Thesis in Geological-mineralogical Sciences, IGGD, St Petersburg, 2000
164. V A Kuznetsov, in *Gidrotermal'nyi Sintez Kristallov* (Hydrothermal Synthesis of Crystals) (Ed. A N Lobachev) (Moscow: Nauka, 1968) p. 77
165. J V Walther, B J Wood, in *Advances in Physical Geochemistry. Fluid–Rock Interactions during Metamorphism* Vol. 5 (Eds J V Walther, B J Wood) (Berlin: Springer, 1986) p. 194
166. G Bliznakov, E Kirkova, K Nikolayeva *Krist. Tech.* **6** (1) 33 (1971)
167. E B Treivus *Kinetika Rosta i Rastvoreniya Kristallov* (Kinetics of Crystal Growth and Dissolution) (Leningrad: Leningrad State University, 1979)

168. V Kitamura, A Kouchi, S Hosoya, I Sunagawa *Mineral J.* **11** (3) 119 (1982)
169. E B Treivus *Vestn. Leningr. Univ., Ser. 7* (7) 17 (1987)
170. C Balarew *Z. Kristallogr.* **181** (1–4) 35 (1987)
171. R D Shannon *Acta Crystallogr., Sect. A* **32** 751 (1976)
172. D V Kalinin *Dokl. Akad. Nauk SSSR* **172** 1167 (1967) [e]
173. R Milke *Am. Mineral.* **89** 211 (2004)
174. A A Chernov, J Lewis *J. Phys. Chem. Solids* **28** 2185 (1967)
175. Yu A Baikov, Yu V Zelenev, W Haubenreisser, H Pfeiffer *Phys. Status Solidi A* **61** 435 (1980)
176. E B Treivus *Vestn. S.-Pb. Univ., Ser. 7* (15) 14 (2000)
177. T Swenson, J E Ricci *J. Am. Chem. Soc.* **61** 1974 (1939)

[a] — *Physics Uspekhi (Engl. Transl.)*
[b] — *J. Exp. Theor. Phys. (Engl. Transl.)*
[c] — *Crystallogr. Rep. (Engl. Transl.)*
[d] — *J. Struct. Chem. (Engl. Transl.)*
[e] — *Dokl. Phys. Chem. (Engl. Transl.)*
[f] — *Bull. Russ. Acad. Sci., Phys. (Engl. Transl.)*